

RECEIVED: June 29, 2022

REVISED: August 27, 2022

ACCEPTED: September 23, 2022

PUBLISHED: October 7, 2022

Effect of spacetime dimensions on quantum entanglement between two uniformly accelerated atoms

Jiatong Yan and Baocheng Zhang¹

*School of Mathematics and Physics, China University of Geosciences,
Wuhan 430074, China*

E-mail: jiatongyan1106@gmail.com, zhangbc.zhang@yahoo.com

ABSTRACT: We investigate the entanglement dynamics for a quantum system composed of two uniformly accelerated Unruh-DeWitt detectors in different spacetime dimensions. It is found that the range of parameters in which entanglement can be generated is shrunk and the amount of generated entanglement is also decreased with the increasing spacetime dimension, by calculating the evolution of two-atom states using the method for open quantum systems. We study the entanglement evolution between two accelerated atoms for different initial two-atom states, and the influence of corresponding spacetime dimensions for every initial state is discussed. When the spacetime dimensions increase, the change of entanglement becomes slower with time. The influence of spacetime dimensions on the change of entanglement also expands to the case of the massive field. The time delay for entanglement generation is shown in different spacetime dimensions. In particular, entanglement decreases more quickly with the increasing spacetime dimensions compared with that in the case of the massless field. The recently found anti-Unruh effect is discussed, and a novel and interesting phenomenon is found that the Unruh effect in small spacetime dimensions can become the anti-Unruh effect in large spacetime dimensions with the same parameters.

KEYWORDS: Thermal Field Theory, Models of Quantum Gravity, Quantum Dissipative Systems

ARXIV EPRINT: [2206.13681](https://arxiv.org/abs/2206.13681)

¹Corresponding author.

Contents

1	Introduction	1
2	Wightman functions and power spectrum	3
2.1	Wightman functions	3
2.2	Power spectrum	4
2.2.1	Diagonal components	4
2.2.2	Off-diagonal components	6
3	Entanglement dynamics in any dimensions	8
3.1	Master equation	8
3.2	Measure for two-atom quantum entanglement	9
3.3	Entanglement change for initial product states	10
3.4	Entanglement change for initial entangled states	16
4	Massive field	18
4.1	Wightman function and power spectrum	18
4.2	Entanglement change	21
5	Conclusion	23

1 Introduction

When studying black hole evaporation, Unruh found that a uniformly accelerating observer in the Minkowski vacuum with acceleration a would perceive a thermal bath of particles with the temperature $T = \hbar a / 2\pi c k_B$ [1–3], which is dubbed as Unruh effect. Since then, it has been extended to many different situations (see the review [4] and references therein). Some of them are related to the physical effects such as the dynamic Casimir effect [5–7], the Lamb shifts [8, 9], the resonance interactions [10, 11] and so on.

Another closely related physical phenomenon influenced by the Unruh effect is quantum entanglement. For a maximally entangled bipartite quantum state, it was found that the state would become less entangled [12] and even sudden death [13] to an observer in relative acceleration. The decrease of entanglement in these and other cases [14–21] could attribute to the fact that accelerating observers only have partial access to the information encoded in the quantum entanglement. However, several studies [22–24] based on the famous Unruh-DeWitt detector model [25] have found that quantum entanglement could be enhanced by the Unruh effect when coupling one or two detectors into the local quantum fields even if they were spacelike separated. This entanglement enhancement is speculated to be extracted from the quantum entanglement of vacuum with which the accelerated

detectors interacted, by a mechanism called entanglement harvesting [26–30]. But these enhancement phenomena didn’t represent a stationary mechanism.

A recent study called as the anti-Unruh effect [31] can provide a stationary mechanism [32] for entanglement enhancement. The anti-Unruh effect means that a uniformly accelerating particle detector may cool down in certain conditions, opposite to the normal Unruh effect. It has been shown to represent a general stationary mechanism that can exist under a stationary state satisfying the Kubo-Martin-Schwinger (KMS) condition [33–35] and is independent on any kind of boundary conditions [31, 32]. A recent calculation showed that the anti-Unruh effect can lead to an increase in the quantum entanglement for the bipartite [36–38] and many-body [39] quantum states. The experimental feasibility of testing the anti-Unruh effect was theoretically analyzed using this multi-body state accelerated in the thermal environment [40, 41]. Interestingly, the anti-Unruh effect can be applied to Banados-Teitelboim-Zanelli (BTZ) black holes [42] and presented a novel phenomenon called the anti-Hawking phenomena [43, 44].

It is noted that all these works listed above about the fascinating change of entanglement induced by the acceleration were discussed in the 2 or 4 spacetime dimensions. But the response function of the accelerated detector in the vacuum, which is crucial for calculating the change of entanglement, is dependent on the number of spacetime dimensions [47, 48]. In even spacetime dimensions, an accelerating observer would feel a Bose-Einstein distribution for the Bosonic field and a Fermi-Dirac distribution for the Fermionic field, which are consistent with our intuition. Under the meaning of statistic inversion by S. Takagi [47], in odd dimensions, the observer would feel a Bose-Einstein distribution for the Fermionic field and a Fermi-Dirac distribution for the bosonic field. This counter-intuitive phenomenon is interesting but it has not been fully understood because of the relativity of the notion of acceleration. Some studies relevant to the statistical inversion by the acceleration have been discussed, including 2-dimensional anyon field [49], geometric phase [50, 51], and fisher information [52]. Methods of optical lattice were used to simulate the Unruh effect in different spacetime dimensions, and evident statistical inversion from Fermi-Dirac to Bose-Einstein in 2-dimensional optical lattice with fermion gas might be observed, which could be a future method to detect the statistic inversion experimentally [53, 54]. A recent study investigated the thermal nature of the Unruh effect in arbitrary dimensions using open quantum systems [55, 56] coupled to massless Minkowski vacuum [57], in which the relationship between the Unruh effect and the thermal bath was also explored. In particular, it was pointed out that the case for the massive field is quite different from the massless field because the statistical factor would disappear [47, 57].

As far as we know, all studies about statistical inversion are restricted to a single-atom system, and the entanglement behavior between two-atom systems in any spacetime dimension has not been investigated up to now. In this paper, based on Gorini-Kossakowski-Linblad-Sudarshan master equation [55], we will study entanglement dynamics of two-atom system in different dimensions. Meanwhile, the different initial states including the product and entangled states for the two-atom system are considered, and the massless and massive fields for the vacuum are also discussed in our paper.

This paper is organized as follows. In the second section, we investigate the model of quantum field theory for the Unruh effect and the theory of open quantum systems. We

also give the concrete Wightman functions and their Fourier transform in any spacetime dimensions and analyze their behavior. This is followed in the third section by the evolution equations and concrete behavior in different parameter conditions for the accelerated two-atom system. The possible anti-Unruh effect is discussed in this section. In the fourth section, we consider the case for the massive field and compare it with the massless field case. Finally, we summarize and give all conclusions in the fifth section. In all calculations of this paper, we take the natural units $\hbar = c = k_B = 1$, where \hbar is the reduced Planck constant, c is the speed of light, and k_B is the Boltzmann constant. In all figures of this paper, we using the dimensionless parameters for the axes under the natural units.

2 Wightman functions and power spectrum

In this section, we will discuss the Wightman functions and their Fourier transform (power spectrum) for the massless field, and analyze their concrete function form, and behavior with the change of ω .

2.1 Wightman functions

The Unruh-DeWitt detector is an idealized model that captures all important features of quantum field theory for describing the Unruh effect. Consider the detector using a two-level atom with ground $|g\rangle$ and excited $|e\rangle$ states which are separated by an energy gap ω .

The Wightman function (sometimes also called correlation functions or two-point functions) for the massless Minkowski field can be written as [47]

$$G(x, x') = \mathcal{C}_D \left[(-1) \left((t - t' - i\epsilon)^2 - |x - x'|^2 \right) \right]^{-(D-2)/2}, \quad (2.1)$$

where D represents the spacetime dimensions, $\epsilon \rightarrow 0^+$, $\mathcal{C}_D = \frac{\Gamma((D-2)/2)}{4\pi^{(D/2)}}$ and Γ stands for the Gamma function. When the two atoms accelerate, their trajectories can be expressed as

$$\begin{aligned} t_1(\tau) &= \frac{1}{a} \sinh a\tau, x_1^1(\tau) = \frac{1}{a} \cosh a\tau, x_1^2 = x_1^3 = \dots = x_1^{D-2}, x_1^{D-1} = 0, \\ t_2(\tau) &= \frac{1}{a} \sinh a\tau, x_2^1(\tau) = \frac{1}{a} \cosh a\tau, x_2^2 = x_2^3 = \dots = x_2^{D-2}, x_2^{D-1} = L, \end{aligned} \quad (2.2)$$

where L is the fixed separation between two atoms along the $(D-1)$ coordinate. For this, the spacetime dimension should be $D \geq 3$ in our consideration.

If the field state satisfies the KMS condition, one has [32, 47]

$$G^{(\alpha\varrho)}(\tau, \tau') = G^{(\alpha\varrho)}(\tau - \tau'), \quad (2.3)$$

which implies that the Wightman function is stationary and depends only on the difference between its two arguments. Inserting eqs. (2.2) and (2.3) into eq. (2.1), the diagonal components are obtained as

$$G^{(11)}(x, x') = G^{(22)}(x, x') = \mathcal{C}_D \left(\frac{a}{2i} \right)^{D-2} \left[\sinh \left(\frac{a\tau}{2} - i\epsilon \right) \right]^{-(D-2)} \quad (2.4)$$

and the off-diagonal components are obtained as

$$G^{(12)}(x, x') = G^{(21)}(x, x') = \mathcal{C}_D \left(\frac{a}{2i} \right)^{D-2} \left[\sinh \left(\frac{a\tau}{2} - i\epsilon \right)^2 - \frac{a^2 L^2}{4} \right]^{-(D-2)/2} \quad (2.5)$$

2.2 Power spectrum

The power spectrum is actually the Fourier transform of Wightman functions, and it has four components in total. We discuss them with the diagonally components and off-diagonally components, respectively.

2.2.1 Diagonal components

The power spectrum of (2.4) can be expressed as

$$\mathcal{G}^{(a)} = \mathcal{C}_D \left(\frac{a}{2i} \right)^{D-2} \int_{-\infty}^{\infty} d\tau e^{-i\omega\tau} \sinh \left(\frac{a\tau}{2} - i\epsilon \right)^{-(D-2)}, \quad (2.6)$$

where $\mathcal{G}^{(a)} \equiv \mathcal{G}^{(11)} = \mathcal{G}^{(22)}$. We slightly downward the integration contour by $i\pi/a$ in such a way that the integrand does not blow up in the singularity along the contour. Then, we get

$$\mathcal{G}^{(a)} = \mathcal{C}_D \left(\frac{a}{2i} \right)^{D-2} \int_{-\infty - \frac{i\pi}{2a}}^{\infty - \frac{i\pi}{2a}} d\tau e^{-i\omega\tau} \sinh \left(\frac{a\tau}{2} \right)^{-(D-2)}. \quad (2.7)$$

Make a variable substitution by $z = e^{a\tau + i\pi}$, and obtain

$$\mathcal{G}^{(a)} = \mathcal{C}_D \frac{1}{a} \int_0^{\infty} dz \frac{z^{\frac{i\omega}{a} + \frac{D-2}{2} - 1}}{(1+z)^{D-2}}. \quad (2.8)$$

Using the Beta function [58]

$$B(p, q) = \int_0^{\infty} dz \frac{z^{p-1}}{(1+z)^{p+q}} = \frac{\Gamma(p)\Gamma(q)}{\Gamma(p+q)}, \quad (2.9)$$

and letting $p = \frac{i\omega}{a} + \frac{D-2}{2}$, $q = \frac{-i\omega}{a} + \frac{D-2}{2}$, we obtain

$$\mathcal{G}^{(a)} = \mathcal{C}_D e^{-\frac{\pi\omega}{a}} \frac{1}{a} \frac{\Gamma\left(\frac{i\omega}{a} + \frac{D-2}{2}\right) + \Gamma\left(\frac{-i\omega}{a} + \frac{D-2}{2}\right)}{\Gamma(D-2)}. \quad (2.10)$$

By the formula $\Gamma(x+iy)^2 = \Gamma(x+iy)\Gamma(x-iy)$ [58], the power spectrum is simplified into

$$\mathcal{G}^{(a)} = \mathcal{C}_D \frac{1}{a} \frac{|\Gamma\left(\frac{D-2}{2} + \frac{i\omega}{a}\right)|^2}{\Gamma(D-2)}. \quad (2.11)$$

In order to present the power spectrum explicitly, the Euler's formulae $|\Gamma(ix)|^2 = \pi/(x \sinh(\pi x))$, $|\Gamma(1/2 + ix)|^2 = \pi/\cosh(\pi x)$, and the property of Gamma function $\Gamma(x+1) = (x+1)\Gamma(x)$ [58] are used to obtain the following form,

$$\mathcal{G}^{(a)} = 2\pi\mathcal{C}_D \frac{1}{\Gamma(D-2)} \begin{cases} \frac{a^{D-2}}{\omega} \frac{1}{e^{\frac{2\pi\omega}{a}} - 1} \prod_{l=0}^{(D-4)/2} \left[l^2 + \left(\frac{\omega}{a} \right)^2 \right], & D \text{ is even} \\ a^{D-3} \frac{1}{e^{\frac{2\pi\omega}{a}} + 1} \prod_{l=0}^{(D-5)/2} \left[\left(l + \frac{1}{2} \right)^2 + \left(\frac{\omega}{a} \right)^2 \right], & D \text{ is odd} \end{cases} \quad (2.12)$$

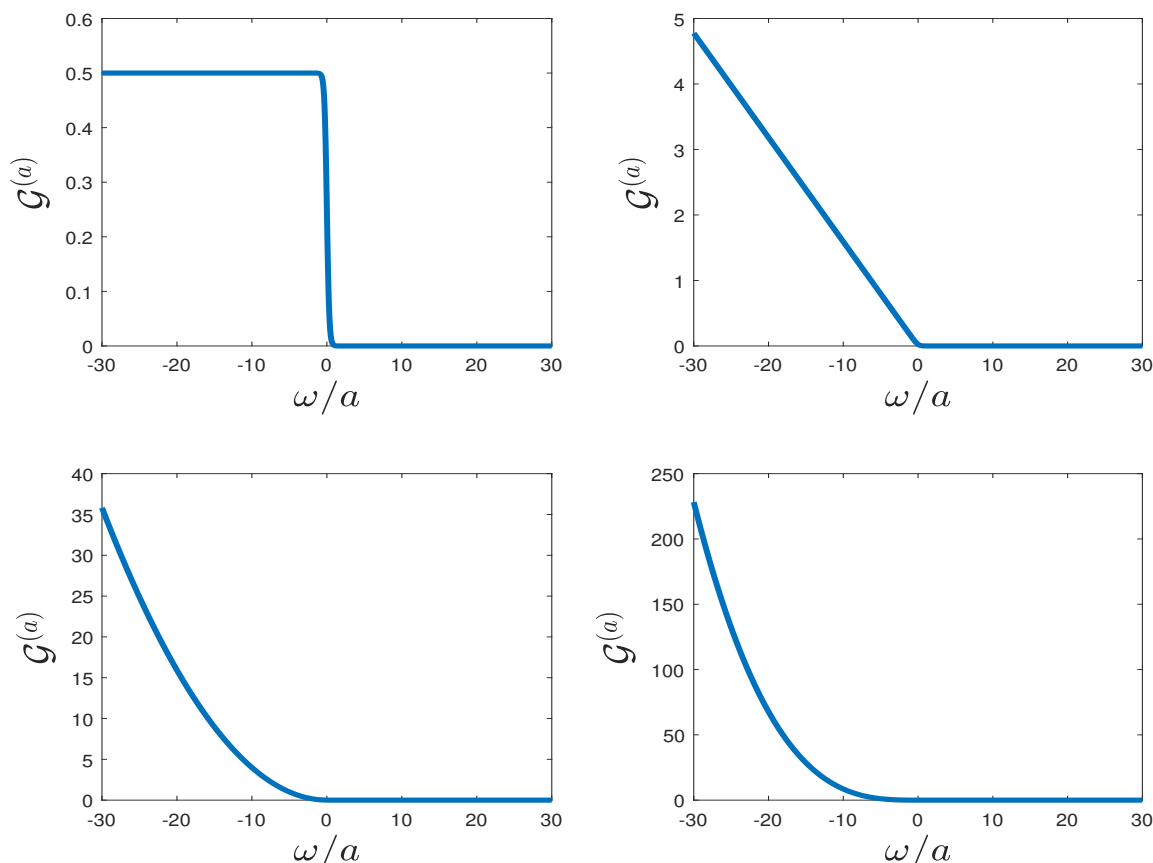


Figure 1. Behavior of $\mathcal{G}^{(a)}$ in different spacetime dimensions. The four subfigures stand for $D = 3$, $D = 4$, $D = 5$, $D = 6$ respectively from left to right and top to bottom.

For the case of the spacetime dimension $D = 3$, the continued product term should be neglected. It is seen a Bose-Einstein factor in even dimensions and a Fermi-Dirac factor in odd dimensions. This is consistent with the Takagi statistical inversion: for Bosonic field, the accelerated observer sees a Bose-Einstein distribution in even spacetime dimensions and a Fermi-Dirac distribution in odd spacetime dimensions. Moreover, it can be inferred directly from eq. (2.12) that the power spectrum $\mathcal{G}^{(a)}$ satisfies the KMS condition [33, 34].

$$\mathcal{G}^{(a)}(\omega) = e^{\frac{-2\pi\omega}{a}} \mathcal{G}^{(a)}(-\omega), \quad (2.13)$$

which means that the ratio between the power spectra with positive and negative frequency is a Boltzmann factor.

The behaviors of the power spectra from $D = 3$ to $D = 6$ are depicted in figure 1. It is noticed that when $\omega > 0$, the value for $\mathcal{G}^{(a)}$ is not zero though very small, and it equals to the product of the corresponding negative frequency value and a Boltzmann factor which restrains the corresponding numerical value, as in eq. (2.13). From figure 1 and eq. (2.12), it is seen that when $D = 3$, $\mathcal{G}^{(a)}$ completely obeys the Fermi-Dirac distribution, which is the most special case; when $D = 4$, $\mathcal{G}^{(a)}$ is equivalent to a product between the inverse of the factor ω and the Bose-Einstein factor; in particular, when $D \geq 5$, the behavior of $\mathcal{G}^{(a)}$ looks all similar since the continued product term would dominate.

2.2.2 Off-diagonal components

Now we calculate the Fourier transform of the off-diagonal components in eq. (2.5) with the expression as

$$\mathcal{G}^{(b)} = \mathcal{C}_D \left(\frac{a}{2i} \right)^{D-2} \int_{-\infty}^{\infty} d\tau e^{-i\omega\tau} \left[\sinh \left(\frac{a\tau}{2} - i\epsilon \right) - \frac{a^2 L^2}{4} \right]^{(D-2)/2}, \quad (2.14)$$

where $\mathcal{G}^{(b)} \equiv \mathcal{G}^{(12)} = \mathcal{G}^{(21)}$. Similar to the calculation of (2.6), slightly downward the integration contour by $i\pi$, and we get

$$\mathcal{G}^{(b)} = \mathcal{C}_D \left(\frac{a}{i} \right)^{D-2} \int_{-\infty-i\pi}^{\infty-i\pi} d\tau e^{-i\omega\tau - \frac{D-2}{2}a\tau} \left[(e^{-a\tau} - e^\gamma) (e^{-a\tau} - e^\beta) \right]^{-(D-2)/2}, \quad (2.15)$$

where $e^\beta = \frac{2+a^2L^2+aL\sqrt{a^2L^2+4}}{2}$ and $e^\gamma = \frac{2+a^2L^2-aL\sqrt{a^2L^2+4}}{2}$. Let $x \equiv a\tau + i\pi$ and we have

$$\mathcal{G}^{(b)} = a^{D-3} e^{\frac{-\pi\omega}{a}} \mathcal{C}_D \int_{-\infty}^{\infty} dx \frac{e^{-i\frac{\omega}{a}x - \frac{D-2}{2}x}}{[e^{-x} + e^\beta]^{\frac{D-2}{2}} [e^{-x} + e^\gamma]^{\frac{D-2}{2}}}. \quad (2.16)$$

Make a further variable substitution, $t = \frac{e^{-\gamma}}{e^x + e^{-\gamma}}$, and the Fourier form becomes

$$\mathcal{G}^{(b)} = a^{D-3} \mathcal{C}_D e^{i\gamma\omega - \frac{D-2}{2}\beta} \int_0^1 dt (1-t)^{\frac{D-2}{2}-i\omega-1} \left[1 - t(1 - e^{\gamma-\beta}) \right]^{-\frac{D-2}{2}} t^{\frac{D-2}{2}-1+i\omega}. \quad (2.17)$$

Using one kind of integration expressions of hypergeometric function [58]

$${}_1F^2(p, q; n, z) = \frac{\Gamma(n)}{\Gamma(q)\Gamma(n-1)} \int_0^1 dt (1-t)^{n-q-1} (1-tz)^{-p} t^{q-1}, \quad (2.18)$$

and letting $p = \frac{D-2}{2}$, $q = \frac{D-2}{2} + i\omega$, $n = D-2$, and $z = 1 - e^{\gamma-\beta}$, we obtain

$$\mathcal{G}^{(b)} = a^{D-3} \mathcal{C}_D e^{i\gamma\omega - \frac{D-2}{2}\beta} \frac{\Gamma\left(\frac{D-2}{2} + i\omega\right) \Gamma\left(\frac{D-2}{2} - i\omega\right)}{\Gamma(D-2)} {}_1F^2\left(\frac{D-2}{2}, \frac{D-2}{2} + i\omega, D-2, 1 - e^{\gamma-\beta}\right). \quad (2.19)$$

Using the same method as we tackle (2.11), an explicit expression for the Fourier form of the off-diagonal components is given as

$$\mathcal{G}^{(b)} = \mathcal{T} \begin{cases} \frac{a^{D-2}}{\omega} \frac{1}{e^{\frac{2\pi\omega}{a}} - 1} \prod_{l=0}^{(D-4)/2} \left[l^2 + (\omega/a)^2 \right], & D \text{ is even} \\ a^{D-3} \frac{1}{e^{\frac{2\pi\omega}{a}} + 1} \prod_{l=0}^{(D-5)/2} \left[\left(l + \frac{1}{2} \right)^2 + (\omega/a)^2 \right], & D \text{ is odd} \end{cases} \quad (2.20)$$

where $\mathcal{T} = 2^{D-5} \Gamma\left(\frac{D-2}{2}\right) {}_1F^2\left(\frac{D-2}{2}, s; D-2, 1 - e^{\gamma-\beta}\right) e^{\gamma p}$, $s = \frac{i\omega}{a} + \frac{D-2}{2}$, $\beta = \log \left[\frac{1}{2} (2 + a^2 L^2 + aL\sqrt{a^2 L^2 + 4}) \right]$, $\gamma = -\beta$.

When the spacetime dimensions $D = 3$, the continued product term should be neglected. We can get directly from (2.20) that it still obeys KMS condition, $\mathcal{G}^{(b)}(\omega) = e^{\frac{-2\pi\omega}{a}} \mathcal{G}^{(b)}(-\omega)$. In particular, if we neglect all constant coefficients, $\mathcal{G}^{(b)}$ can be regraded as the multiplication of corresponding $\mathcal{G}^{(a)}$ and a hypergeometric function.

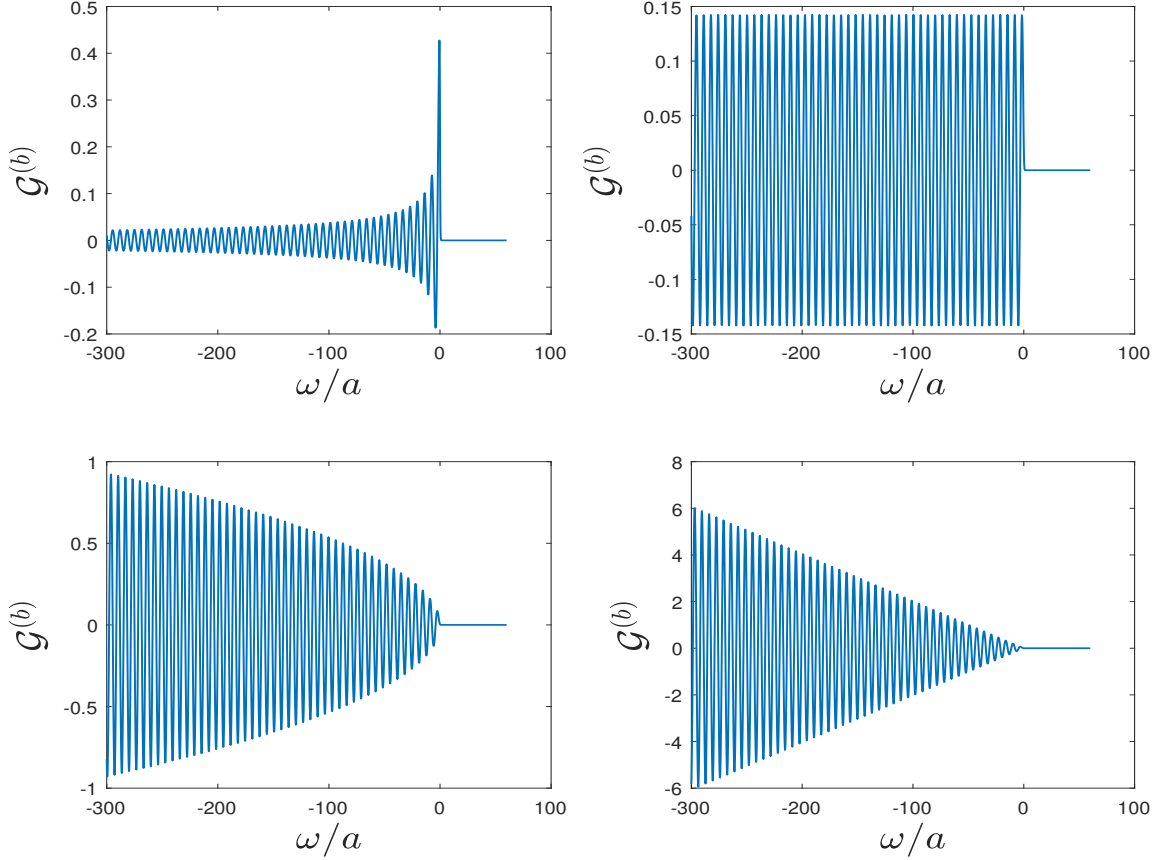


Figure 2. Behavior of $\mathcal{G}^{(b)}$ in different spacetime dimensions. The four subfigures stand for $D = 3$, $D = 4$, $D = 5$, $D = 6$ respectively from left to right and top to bottom.

The behaviors of the power spectra from $D = 3$ to $D = 6$ are depicted in figure 2 with the distance between two atoms $L = 1$. It is seen clearly from figure 2 that for $D = 3$, the value for $\mathcal{G}^{(b)}$ will decrease by an oscillating form with ω decreasing from 0 to negative values; for $D = 4$, $\mathcal{G}^{(b)}$ oscillates periodically but the value is not decreasing for $\omega \leq 0$; for $D = 5$ and $D = 6$, $\mathcal{G}^{(b)}$ will oscillate with an inverse trend comparing with the case $D = 3$ although the oscillation for $D = 6$ is more violent than that for $D = 5$. The hypergeometric function term is responsible for the oscillation. These oscillation can be understood from the expression of $\mathcal{G}^{(b)}$. For example, when $D = 4$, the expression for $\mathcal{G}^{(b)}$ can be written as

$$\frac{1}{2\pi} \frac{1}{e^{\frac{2\pi\omega}{a}} - 1} \frac{\sin\left(\frac{2\omega}{a} \sinh^{-1} \frac{aL}{2}\right)}{L\sqrt{1 + a^2 L^2/4}}. \quad (2.21)$$

It is seen that when $\omega < 0$, the Bose-Einstein factor is negligible and the sin function would dominate the oscillation. Thus, the oscillation amplitude would be not changed with the frequency ω for the constant a and L .

3 Entanglement dynamics in any dimensions

In the framework of open quantum systems [55] and with the help of Negativity, we study the relationship between entanglement dynamics and spacetime dimensions in the case of the massless field for the vacuum. The Unruh and anti-Unruh effects are also discussed in this section.

3.1 Master equation

Consider two atoms that consist of two energy levels for each one accelerating in the Minkowski vacuum, and the total Hamiltonian for the interaction process between accelerated atoms and the vacuum field can be written as

$$H = H_A + H_F + H_I. \quad (3.1)$$

H_A is the Hamiltonian of the two-atom system,

$$H_A = \frac{\omega}{2}\sigma_3^{(1)} + \frac{\omega}{2}\sigma_3^{(2)}, \quad (3.2)$$

where $\sigma_i^{(1,2)} = \sigma_i \otimes \sigma_0$, the superscripts (1, 2) indicate the two different atoms, $\sigma_i (i = 1, 2, 3)$ is the Pauli matrices and σ_0 is the 2×2 unit matrix. ω is the energy gap of each atom. H_F is the Hamiltonian of the scalar fields that represents the massless vacuum field. We assume the interaction Hamiltonian H_I is weak, with the following form,

$$H_I = \mu[\sigma_2^{(1)}\phi(t, x_1) + \sigma_2^{(2)}\phi(t, x_2)], \quad (3.3)$$

where μ is the coupling constant which is assumed to be small.

To make the calculation further, some approximations must be taken (see the detailed discussion in ref. [57]). Under the Born-Markov approximation [55], we can write the master equation describing the dissipative dynamics of the two-atom system in the manner of Gorini-Kossakowski-Lindblad-Sudarshan form,

$$\frac{\partial \rho(\tau)}{\partial \tau} = -i[H_{\text{eff}}, \rho(\tau)] + \mathcal{D}[\rho(\tau)] \quad (3.4)$$

where

$$H_{\text{eff}} = H_A - \frac{i}{2} \sum_{\alpha, \beta=1}^2 \sum_{i, j=1}^3 H_{ij}^{(\alpha\beta)} \sigma_i^{(\alpha)} \sigma_j^{(\beta)} \quad (3.5)$$

and

$$\mathcal{D}[\rho(\tau)] = \frac{1}{2} \sum_{\alpha, \beta=1}^2 \sum_{i, j=1}^3 C_{ij}^{(\alpha\beta)} \left[2\sigma_j^{(\beta)} \rho \sigma_i^{(\alpha)} - \sigma_i^{(\alpha)} \rho \sigma_j^{(\beta)} - \rho \sigma_i^{(\alpha)} \sigma_j^{(\beta)} \right] \quad (3.6)$$

From the master equation (3.4), it is clear that the environment can lead to dissipation and decoherence defined by the dissipator $\mathcal{D}[\rho(\tau)]$, and the coefficients $C_{ij}^{(\alpha\beta)}$ in the dissipator is expressed as

$$C_{ij}^{(\alpha\beta)} = A^{(\alpha\beta)} \delta_{ij} - iB^{(\alpha\beta)} \varepsilon_{ijk} \delta_{3k} - A^{(\alpha\beta)} \delta_{3i} \delta_{3j} \quad (3.7)$$

where

$$\begin{aligned} A^{(\alpha\beta)} &= \frac{\mu^2}{4} \left[\mathcal{G}^{(\alpha\beta)}(-\omega) + \mathcal{G}^{(\alpha\beta)}(\omega) \right] \\ B^{(\alpha\beta)} &= \frac{\mu^2}{4} \left[\mathcal{G}^{(\alpha\beta)}(-\omega) - \mathcal{G}^{(\alpha\beta)}(\omega) \right] \end{aligned} \quad (3.8)$$

and the concrete expression for $\mathcal{G}^{(\alpha\beta)}$ can be found in eqs. (2.12) and (2.20). $H_{ij}^{(\alpha\beta)}$ is the Hilbert transform of corresponding power spectrum $G_{ij}^{(\alpha\beta)}$,

$$\mathcal{K}^{(\alpha\beta)}(\lambda) = \frac{1}{\pi i} P \int_{-\infty}^{\infty} d\omega \frac{G_{ij}^{(\alpha\beta)}(\omega)}{\omega - \lambda}, \quad (3.9)$$

where P denoting the Cauchy principle value. It is noted that the eqs. (3.8) and (3.9) depends on the entire history of the detector, which looks contrary to the present discussion about the time evolution of the state density. This is due to the Markovian approximation made in the master equation, which enables integration limits for some terms (related to the Wightman functions) can be taken to infinite proper time since the integrand disappears for the large time over which the field correlation function decay sufficiently fast. More detailed interpretation refers to ref. [57]. Moreover, in this paper we just consider the effect of environment (the vacuum field) on quantum entanglement between two accelerated atoms in arbitrary dimensions, so the Hamiltonian for any single atom and vacuum contribution terms can be neglected, and we just need to consider the effect of dissipator $\mathcal{D}(\rho(\tau))$.

3.2 Measure for two-atom quantum entanglement

For convenience, we choose four Dicke states [59] as the bases for the expression of density matrix,

$$\begin{aligned} |e\rangle &= |e_1\rangle \otimes |e_2\rangle, \\ |s\rangle &= (|g_1\rangle \otimes |e_2\rangle + |g_2\rangle \otimes |e_1\rangle) / \sqrt{2}, \\ |g\rangle &= |g_1\rangle \otimes |g_2\rangle, \\ |a\rangle &= (|g_1\rangle \otimes |e_2\rangle - |g_2\rangle \otimes |e_1\rangle) / \sqrt{2}. \end{aligned} \quad (3.10)$$

The density matrix of the system can be written as

$$\rho(t) = \begin{bmatrix} \rho_{ee}(t) & \rho_{eg}(t) & 0 & 0 \\ \rho_{eg}^*(t) & \rho_{gg}(t) & 0 & 0 \\ 0 & 0 & \rho_{ss}(t) & 0 \\ 0 & 0 & 0 & \rho_{aa}(t) \end{bmatrix} \quad (3.11)$$

where $\rho_{IJ} = \langle I | \rho | J \rangle$, $I, J = e, s, g, a$. We take Negativity as measurement in order to define the entanglement amount of the two-atom system.

Negativity is an important measure for entanglement, it is defined [60, 61] according to

$$\mathcal{N} = \max \left\{ 0, -2 \sum_i \mu_i \right\} \quad (3.12)$$

where μ_i are the eigenvalues of the partial transposition [62, 63] of the density matrix ρ of two-body system. It is not hard to confirm that $\mathcal{N} = 0$ for unentangled states of atoms and $\mathcal{N} = 1$ for maximally entangled states of atoms. Using the density matrix (3.11), the Negativity is obtained as

$$\mathcal{N} = \max \{0, \mathcal{N}_1, \mathcal{N}_2\} \quad (3.13)$$

where

$$\begin{aligned} \mathcal{N}_1 &= \sqrt{\mathcal{C}_1 \mathcal{C}_1^+ + (\rho_{gg} + \rho_{ee})^2} - (\rho_{gg} + \rho_{ee}), \\ \mathcal{N}_2 &= \sqrt{\mathcal{C}_2 \mathcal{C}_2^+ + (\rho_{aa} + \rho_{ss})^2} - (\rho_{aa} + \rho_{ss}), \\ \mathcal{C}_1 &= |\rho_{aa} - \rho_{ss}| - 2\sqrt{\rho_{gg} - \rho_{ee}}, \\ \mathcal{C}_2 &= 2|\rho_{ge}| - (\rho_{ss} + \rho_{aa}), \\ \mathcal{C}_1^+ &= |\rho_{aa} - \rho_{ss}| + 2\sqrt{\rho_{gg} - \rho_{ee}}, \\ \mathcal{C}_2^+ &= 2|\rho_{ge}| + (\rho_{ss} + \rho_{aa}). \end{aligned} \quad (3.14)$$

3.3 Entanglement change for initial product states

Combining (3.11) with (3.4), we can get a set of differential equations

$$\begin{aligned} \rho'_{gg} &= -4(A_a - B_a)\rho_{gg} + 2(A_a + B_a - A_b - B_b)\rho_{aa} + 2(A_a + B_a + A_b + B_b)\rho_{ss}, \\ \rho'_{ee} &= -4(A_a + B_a)\rho_{ee} + 2(A_a - B_a - A_b + B_b)\rho_{aa} + 2(A_a - B_a + A_b - B_b)\rho_{ss}, \\ \rho'_{aa} &= -4(A_a - A_b)\rho_{aa} + 2(A_a - B_a - A_b + B_b)\rho_{gg} + 2(A_a + B_a - A_b - B_b)\rho_{ee}, \\ \rho'_{ss} &= -4(A_a + A_b)\rho_{ss} + 2(A_a - B_a + A_b - B_b)\rho_{gg} + 2(A_a + B_a + A_b + B_b)\rho_{ee}, \\ \rho'_{ge} &= -4A_a\rho_{ge}, \quad \rho'_{eg} = -4A_a\rho_{eg}, \end{aligned} \quad (3.15)$$

where $\rho'_{IJ} = \frac{\partial \rho_{IJ}(\tau)}{\partial \tau}$, and the parameters A and B are defined in eq. (3.8) with the corresponding concise signs here, $A_a \equiv A^{(11)} = A^{(22)}$, $A_b \equiv A^{(12)} = A^{(21)}$, $B_a \equiv B^{(11)} = B^{(22)}$, and $B_b \equiv B^{(12)} = B^{(21)}$.

In order to study the generation of entanglement, we choose the initial state to be a product state $|10\rangle$, without loss of generality. From eq. (3.10), it is easy to deduce that $\rho_{eg} = \rho_{ge}$ remains zero during the whole process, which leads to the result that \mathcal{N}_2 in eq. (3.13) is always negative. Thus, the Negativity can be calculated according to

$$\mathcal{N}(\rho(\tau)) = \max(0, \mathcal{N}_1(\tau)) \quad (3.16)$$

From (3.15) and (3.16), we can get the expression for the derivative value of Negativity $\mathcal{N}_1(\tau)$ at $\tau = 0$,

$$\mathcal{N}'_1(0) = k \left(4|A_b^2| - 4\sqrt{A_a^2 - B_a^2} \right) \quad (3.17)$$

where k is a coefficient related to the spacetime dimensions D , the acceleration a , the difference ω of energy levels of atom and the separation between atoms L , and k is always

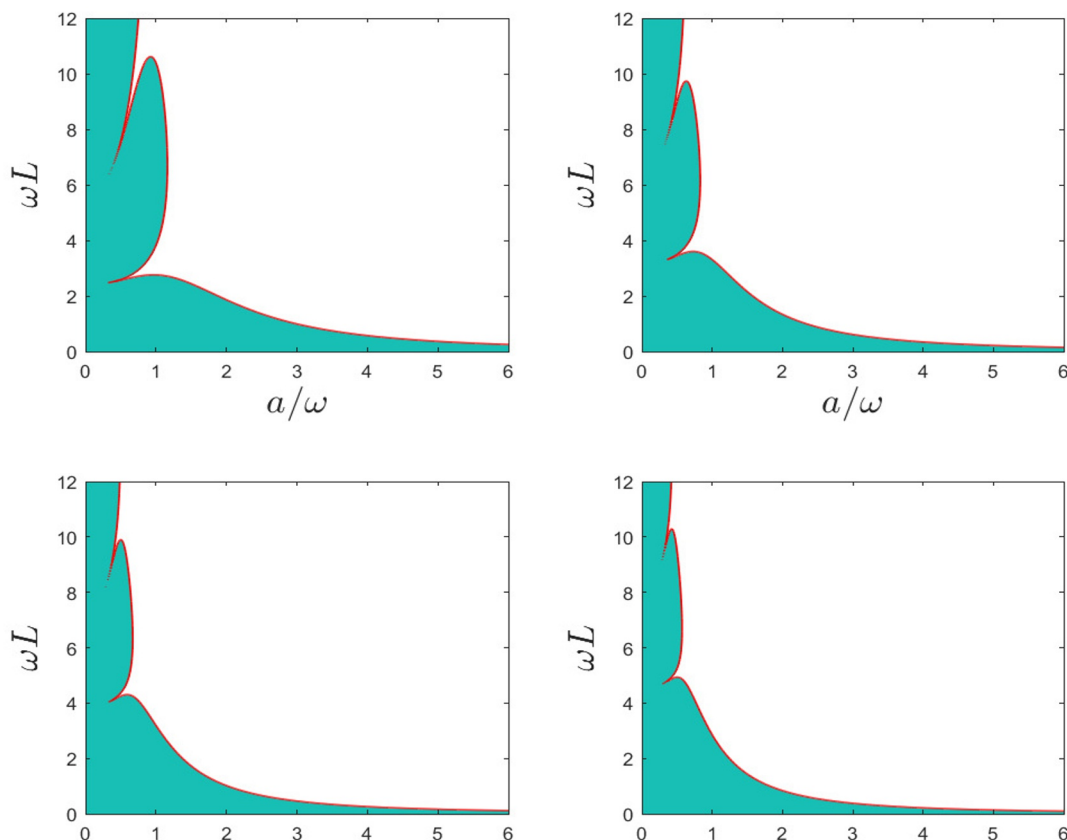


Figure 3. Entanglement region in the $a - L$ plane. The four subfigures stand for $D = 3$, $D = 4$, $D = 5$, $D = 6$ respectively from left to right and top to bottom.

positive. If $\mathcal{N}'_1(0) > 0$, it is deduced that entanglement is produced at the neighborhood of the initial time.

In the following part, we will investigate how large it is for the region of different parameters (a, ω, L) in which entanglement could be generated in different spacetime dimensions.

At first, we study the region where entanglement could be generated in the $a - L$ plane with the dimensionless parameters for the axes, as presented in figure 3. The areas of presented entanglement regions are estimated as 17.38, 13.63, 11.88, and 10.80 for $D = 3$, $D = 4$, $D = 5$, $D = 6$, respectively. It is stressed that the numerical values for the entanglement area don't have the physical meaning, and it only indicates that the larger the area is, the larger it is for the range of considered parameters with which entanglement can be generated between atoms. It is not hard to find from figure 3 that the area of the entanglement region in the $a - L$ plane would decrease with the increasing spacetime dimensions. And we have calculated the area of entanglement region for the same D but different ω , and found that the larger ω is, the larger the area is.

Then, we investigate the entanglement-generated region in the $\omega - a$ plane with the dimensionless parameters for the axes, as presented in figure 4. The areas of entanglement

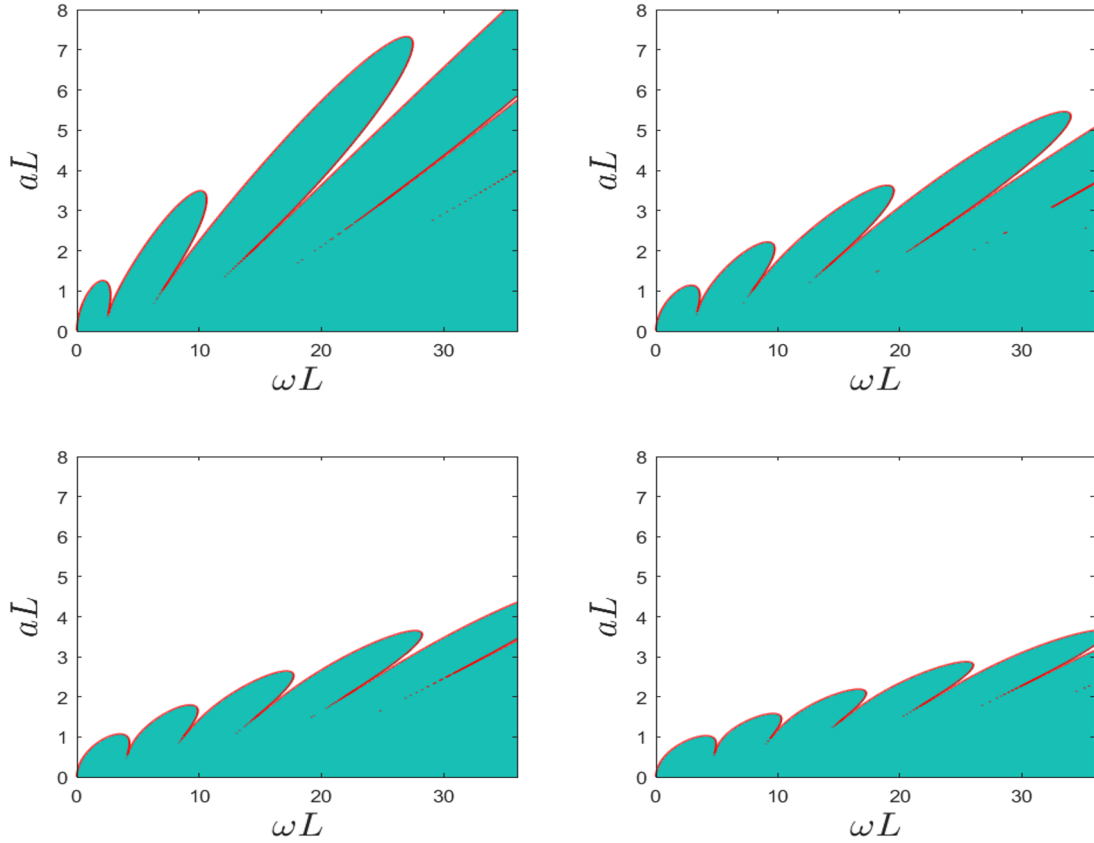


Figure 4. Entanglement region in the $\omega - a$ plane. The four subfigures stand for $D = 3$, $D = 4$, $D = 5$, $D = 6$ respectively from left to right and top to bottom.

regions are estimated as 116.17, 113.88, 90.45, and 77.58 for $D = 3$, $D = 4$, $D = 5$, $D = 6$, respectively. Similar to the $a - L$ figure in figure 3, the area of the entanglement region in the $\omega - a$ plane is decreasing with the increasing spacetime dimensions. And we have calculated the area of entanglement region for the same D but different L , and find that the smaller L is, the larger the area is.

Finally, we investigate the entanglement-generated region in the $\omega - L$ plane with dimensionless parameters for the axes, as presented in figure 5. Similarly, we calculate the areas of entanglement regions as 108.67, 72.93, 38.76 and 22.06 for $D = 3$, $D = 4$, $D = 5$, $D = 6$, respectively. It is found that the area of entanglement region in the $\omega - L$ plane is decreasing with the increasing spacetime dimensions. And we have calculated the area of entanglement region for the same D but different a , and find that the smaller a is, the larger the area is.

We make some discussions for figure 3, figure 4 and figure 5. From all the three figures, it is seen that for larger spacetime dimensions, the range of the parameters (a, ω, L) in which entanglement can be generated is decreasing. According to the calculation, we can give some interpretations. From the theory of the master equation, the change of entanglement is derived from a similar effect to that environment induced entanglement change. Here the vacuum in different spacetime dimensions can be regarded as the environment. When the

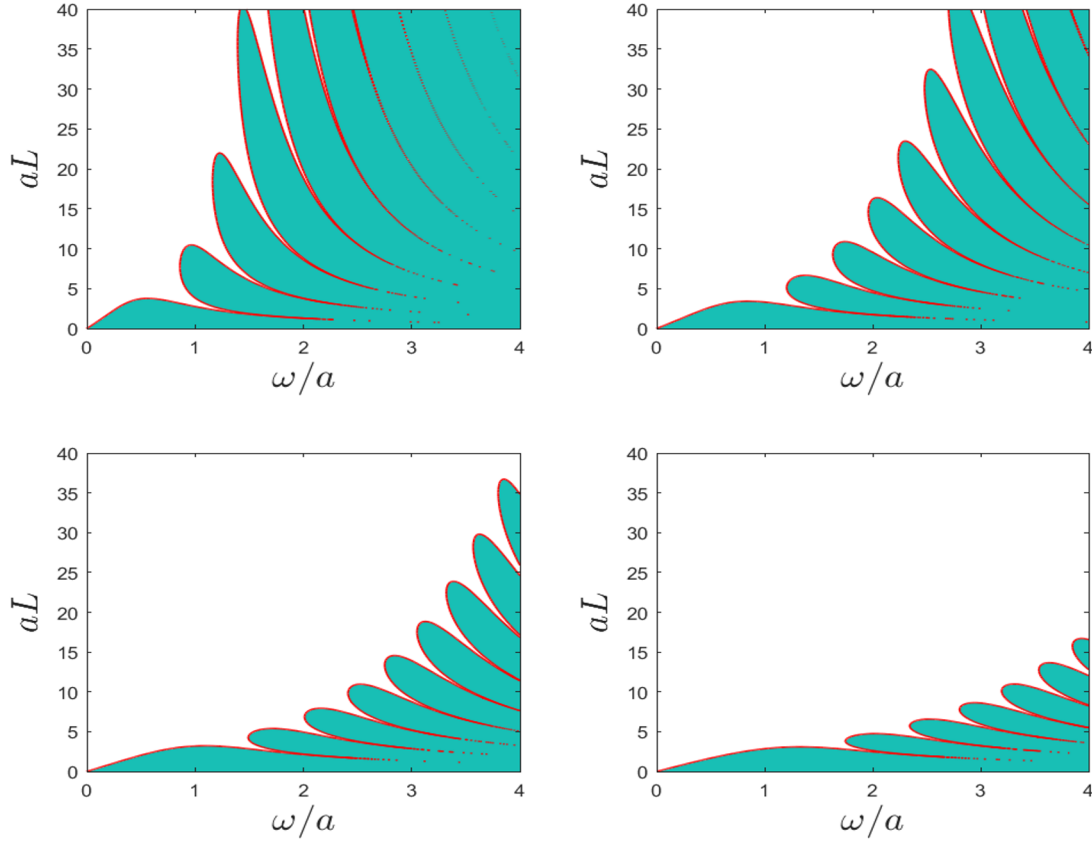


Figure 5. Entanglement region in the $\omega - L$ plane. The four subfigures stand for $D = 3$, $D = 4$, $D = 5$, $D = 6$ respectively from left to right and top to bottom.

spacetime dimensions increase, the environment would become more sophisticated due to the addition of the spatial dimensions, which can be manifested by our calculation to some extent. It is not hard to understand that the entanglement region becomes smaller when the separation between atoms or the acceleration increases, which means that the increased parameters (L, a) would lead to the increase of difficulty for the generation of entanglement. It is a little surprised that the entanglement region increases when the energy level of the atom increases. More careful investigation finds that the entangled value measured by Negativity would decrease for increasing energy level of the atom although the area of the entanglement region increases.

Furthermore, if we combine the KMS condition (2.13) with eq. (3.17), another condition for the entanglement region can be expressed as

$$\left| \left(1 + e^{\frac{2\pi\omega}{a}} \right) \mathcal{G}^{(b)}(-\omega) \right| - 2e^{\frac{\pi\omega}{a}} \mathcal{G}^{(a)}(-\omega) > 0, \quad (3.18)$$

which leads to a more refined result that the entanglement region is not simply connected. For example, we fix $D = 4$, and check the partially amplified entanglement region in the $a - L$ plane, as given in figure 6. It is found that there are many small holes where entanglement would not be generated. This reason is that there is no evident boundary between entanglement region and no-entanglement region, which can be deduced by the fact that the $\mathcal{G}^{(b)}(-\omega)$ term in (3.18) is oscillating with a or L (such oscillating behaviors cannot

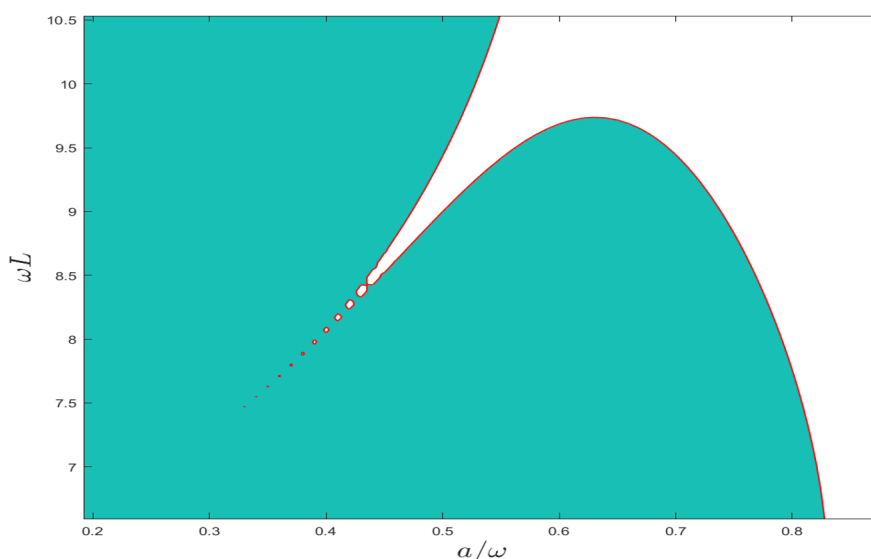


Figure 6. Partially amplified figure of the $D = 4$ case of figure 3.

be presented using the figures but it can be observed only by the analyzed expressions in the second section) but $\mathcal{G}^{(a)}(-\omega)$ term is monotonous with a or L .

Now we discuss the change of entanglement generated after atoms are accelerated with time in different spacetime dimensions. Figure 7 presents this evolution by calculating the amount of Negativity with the parameters $L = 1$, $\omega = 1$. It is seen clearly that when the spacetime dimension is smaller, entanglement is generated more quickly but decays also more quickly. Meanwhile, when the spacetime dimension decreases, the maximal value of entanglement increases, but the entanglement duration time (this is estimated by the half-width of the evolution curves) decreases.

Figure 8 presents the change of maximal values of generated entanglement using Negativity with a throughout the whole evolved process. We plot different results for different L . It is seen that for small L , the maximum of Negativity will decrease monotonously with increasing acceleration, and for larger spacetime dimensions, entanglement would decrease to zero more quickly. When L increases, the maximum of Negativity would not decrease monotonously but increase first and decrease then to zero, and this phenomenon will happen for smaller L under smaller spacetime dimensions. The increase of entanglement with the increasing acceleration a looks like the phenomena appeared in the case of anti-Unruh effect [31, 36]. We will not discuss this here more detailed, and postpone it to the next section for the case of the massive field. When L takes larger values, the maximum of Negativity will oscillate with increasing acceleration. This oscillation is interesting but there is not an explicit interpretation for it, which might deserve to be studied further in the future. Moreover, it is also noted that the possible generated maximum of entanglement will decreases with the increasing separation between atoms, as expected.

We also calculate the change of maximal values of generated entanglement using Negativity with other parameters (e.g. L or ω) throughout the whole evolved process. The results are similar to that presented in figure 8 and there is not any novel behavior, so we would not discuss these here.

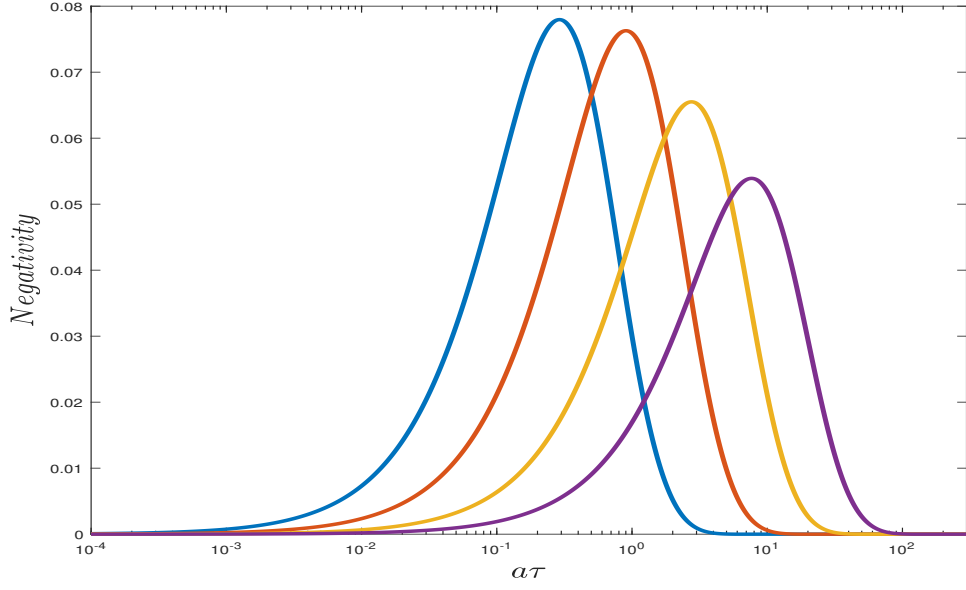


Figure 7. Entanglement evolutionary process over time. Blue, red, yellow and purple lines stand for $D = 3$, $D = 4$, $D = 5$, $D = 6$, respectively.

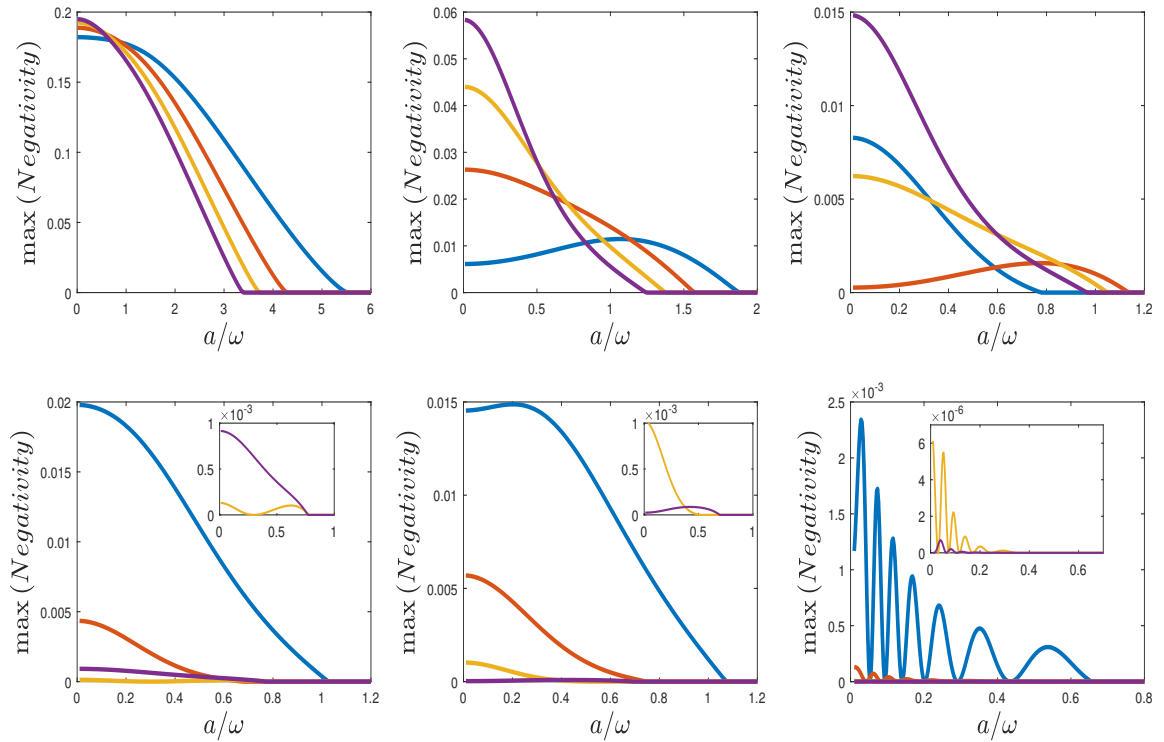


Figure 8. Changes of maximal Negativity with acceleration for different atom separations. The six subfigures stand for $L = 0.3$, $L = 2$, $L = 3$, $L = 4$, $L = 4.4$, and $L = 30$ respectively from left to right and top to bottom. Blue, red, yellow and purple lines stand for $D = 3$, $D = 4$, $D = 5$, and $D = 6$, respectively.

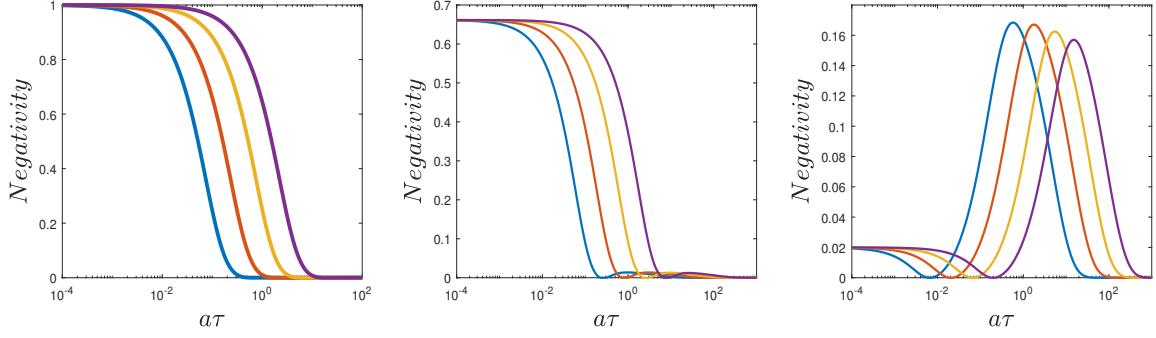


Figure 9. Entanglement evolutionary process over time for different initial entangled states. The three subfigures stand for $\alpha = 1/\sqrt{2}$, $\alpha = 1/(2\sqrt{2})$, $\alpha = 0.01$, respectively, from left to right.

3.4 Entanglement change for initial entangled states

In this section, we study the change of entanglement with the initial entangled states, $\alpha|10\rangle + \beta|01\rangle$ ($\alpha, \beta \neq 0, \alpha^2 + \beta^2 = 1$). Figure 9 presents the change of entanglement with time with the parameters $\omega = 1$, $L = 0.3$. As shown in the left one of figure 9, the amount of entanglement will decrease monotonously with time for initially maximally entangled states. In particular, the larger the spacetime dimension D is, the later it is for time that entanglement disappears. When the initial entanglement is not big enough, it will decrease first to zero, followed by a slight increase, and then decrease to zero finally, as presented in the middle one of figure 9. It is interesting for the small initial entanglement in the right one of figure 9, it decreases to zero at first and then increases to a value larger than the initial entanglement, and the generated maximal entanglement by accelerating two atoms with an initial product state as in figure 7. It seems that the initial small entanglement can boost the generated amount of entanglement by the acceleration. This looks like an amplification mechanism for quantum entanglement, but the amplification will be not valid if the initial amount of entanglement is large enough, as in the middle one of figure 9.

In the following, we discuss the change of entanglement for initial entangled states in two different asymptotic cases, $L \rightarrow \infty$ and $L \rightarrow 0$. At first, we discuss the case with $L \rightarrow \infty$. In this condition, $\mathcal{G}^{(b)} = 0$, $A_b = B_b = 0$. We can analytically solve (3.15) and obtain the corresponding results as

$$\begin{aligned}
 \rho_{aa} &= \frac{A_1^2 - B_1^2 + A_1^2 e^{-8A_1\tau} - B_1^2 e^{-8A_1\tau} - 4A_1^2 \alpha \beta e^{-4A_1\tau} + 2B_1^2 e^{-4A_1\tau}}{4A_1^2} \\
 \rho_{ee} &= \frac{(A_1 - B_1) e^{-8A_1\tau} (-1 + e^{4A_1\tau}) (A_1 + B_1 + A_1 e^{4A_1\tau} - B_1 e^{4A_1\tau})}{4A_1^2} \\
 \rho_{gg} &= \frac{(A_1 + B_1) e^{-8A_1\tau} (-1 + e^{4A_1\tau}) (A_1 - B_1 + A_1 e^{4A_1\tau} + B_1 e^{4A_1\tau})}{4A_1^2} \\
 \rho_{ss} &= \frac{A_1^2 - B_1^2 + A_1^2 e^{-8A_1\tau} - B_1^2 e^{-8A_1\tau} + 4A_1^2 \alpha \beta e^{-4A_1\tau} + 2B_1^2 e^{-4A_1\tau}}{4A_1^2}
 \end{aligned} \tag{3.19}$$

Substituting this into (3.13), Negativity can be given in any time of the evolution progress. It is found that Negativity will decrease rapidly to zero, no matter what initial state or acceleration we choose.

Next, let $L \rightarrow 0$, under which $A_a = A_b$, $B_a = B_b$. We can solve (3.15) analytically and obtain the corresponding results as

$$\rho_{aa} = \frac{1}{2}(\alpha - \beta)^2, \quad (3.20)$$

$$\begin{aligned} \rho_{ee} = & \frac{(1+2\alpha\beta)(A_1-B_1)^2}{6A_1^2+2B_1^2} \\ & - \left((1+2\alpha\beta) \left(-A_1+B_1+\sqrt{(A_1-B_1)(A_1+B_1)} \right) \right) \left(A_1^3-A_1B_1^2+2B_1^2\sqrt{(A_1-B_1)(A_1+B_1)} \right) \\ & + \left((A_1-B_1)(A_1+B_1)^{3/2} \right) e^{-4(2A_1+\sqrt{(A_1-B_1)(A_1+B_1)})\tau} / \left(4B_1\sqrt{(A_1-B_1)(A_1+B_1)}(3A_1^2+B_1^2) \right) \\ & + \left((1+2\alpha\beta) \left(A_1-B_1+\sqrt{(A_1-B_1)(A_1+B_1)} \right) \right) \left(-A_1^3+A_1B_1^2+2B_1^2\sqrt{(A_1-B_1)(A_1+B_1)} \right) \\ & + \left((A_1-B_1)(A_1+B_1)^{3/2} \right) e^{-4(2A_1-\sqrt{(A_1-B_1)(A_1+B_1)})\tau} / \left(4B_1\sqrt{(A_1-B_1)(A_1+B_1)}(3A_1^2+B_1^2) \right), \end{aligned} \quad (3.21)$$

$$\begin{aligned} \rho_{gg} = & \frac{(1+2\alpha\beta)(A_1+B_1)^2}{6A_1^2+2B_1^2} \\ & - \left((1+2\alpha\beta) \left(A_1+B_1-\sqrt{(A_1-B_1)(A_1+B_1)} \right) \right) \left(A_1^3-A_1B_1^2+2B_1^2\sqrt{(A_1-B_1)(A_1+B_1)} \right) \\ & + \left((A_1-B_1)(A_1+B_1)^{3/2} \right) e^{-4(2A_1+\sqrt{(A_1-B_1)(A_1+B_1)})\tau} / \left(4B_1\sqrt{(A_1-B_1)(A_1+B_1)}(3A_1^2+B_1^2) \right) \\ & - \left((1+2\alpha\beta) \left(A_1+B_1+\sqrt{(A_1-B_1)(A_1+B_1)} \right) \right) \left(-A_1^3+A_1B_1^2+2B_1^2\sqrt{(A_1-B_1)(A_1+B_1)} \right) \\ & + \left((A_1-B_1)(A_1+B_1)^{3/2} \right) e^{-4(2A_1-\sqrt{(A_1-B_1)(A_1+B_1)})\tau} / \left(4B_1\sqrt{(A_1-B_1)(A_1+B_1)}(3A_1^2+B_1^2) \right), \end{aligned} \quad (3.22)$$

$$\begin{aligned} \rho_{ss} = & \frac{(1+2\alpha\beta)(A_1^2-B_1^2)}{2(3A_1^2+B_1^2)} + \frac{(1+2\alpha\beta) \left(A_1^2+B_1^2-A_1\sqrt{(A_1-B_1)(A_1+B_1)} \right) e^{-4(2A_1-\sqrt{(A_1-B_1)(A_1+B_1)})\tau}}{2(3A_1^2+B_1^2)} \\ & + \frac{(1+2\alpha\beta) \left(A_1^2+B_1^2+A_1\sqrt{(A_1-B_1)(A_1+B_1)} \right) e^{-4(2A_1+\sqrt{(A_1-B_1)(A_1+B_1)})\tau}}{2(3A_1^2+B_1^2)}. \end{aligned} \quad (3.23)$$

Assume that when $\tau \rightarrow \infty$, the value for Negativity is N . The change of N with respect to ω is shown in figure 10 with the parameter $D = 3$. From this figure, it is found that for a general entangled state initially (see the red line in figure 10), when ω is very small, the Negativity will decrease to zero; after ω increases to some value, N will grow rapidly to a fixed value, but this fixed value is related to the initial states; when ω becomes larger, N will decrease suddenly to zero and keep zero for larger ω . That is to say, if there is no separation between two atoms, entanglement will not disappear within a certain range of

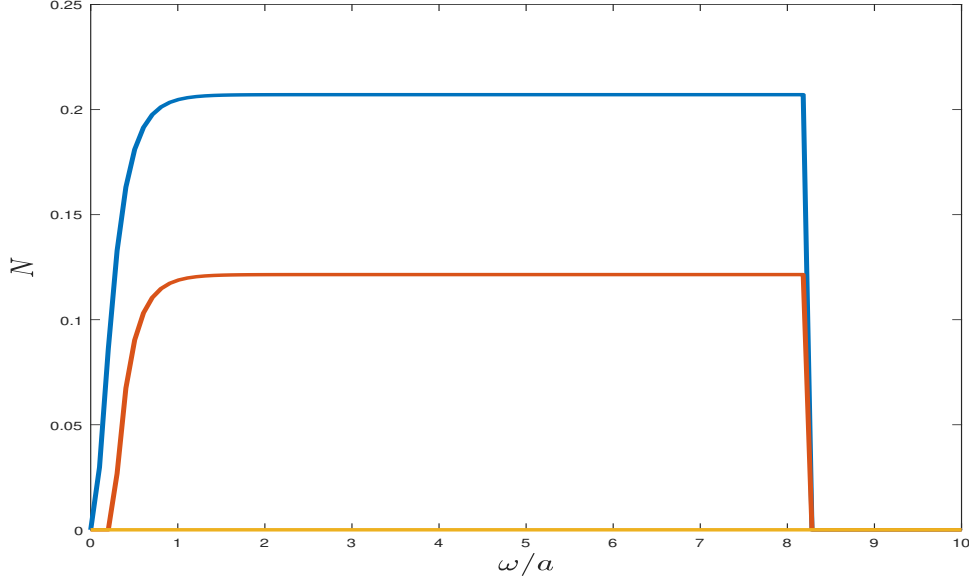


Figure 10. The change of N with ω for different initial states, with $\alpha = 0$ for the blue line, $\alpha = 0.1$ for the red line, and $\alpha = 1/\sqrt{2}$ for the yellow line.

ω , except for the initially maximally entangled state ($\alpha = \beta = \frac{1}{\sqrt{2}}$) where entanglement always remains at zero, as presented with the yellow line in figure 10. In particular, we find that the amount of generated entanglement by the acceleration is maximal if the initial state is a product state ($\alpha = 1$ or $\beta = 1$), as presented with the blue line in figure 10. In particular, when $\tau \rightarrow \infty$, the behaviors of Negativity are nearly the same for the different spacetime dimensions.

4 Massive field

In the last section, we investigate the dynamics of entanglement for two accelerated atoms under the condition that the vacuum field is considered as the massless field. In this section, we will turn to the consideration of a massive field for the vacuum and discuss the influence of acceleration on entanglement under different spacetime dimensions.

4.1 Wightman function and power spectrum

In D -dimensional Minkowski spacetime, the scalar field operator could be expanded as

$$\phi(t, x) = \int d^{D-1}k \frac{1}{\sqrt{2\omega_k 2\pi^{D-1}}} \left[a_k e^{ikx - i\omega_k t} + a_k^\dagger e^{-ikx + i\omega_k t} \right], \quad (4.1)$$

where a_k (a_k^\dagger) is the annihilation (creation) operator. The expression for Wightman function is

$$G^{(\alpha\varrho)}(\Delta t) = \langle \phi(t_\alpha(t), x_\alpha(t)) \phi(t_\varrho(t'), x_\varrho(t')) \rangle, \quad (4.2)$$

where $\Delta t = t - t'$ is the difference of time. Inserting (4.1) into (4.2), one obtains

$$G^{(\alpha\varrho)}(\Delta t) = \frac{1}{(2\pi)^{D-1}} \int d^{D-1}k \frac{1}{2\omega_k} e^{-i\omega_k \Delta t + ikx}. \quad (4.3)$$

Here the integral of $d^{D-1}k$ can be regarded as the integral of the length and the direction of the vector whose direction can be described by $(D-2)$ angular coordinates. After integrating all the angular variables, the Wightman function becomes

$$G^{(\alpha\varrho)}(\Delta t) = \frac{1}{(4\pi)^{\frac{D-1}{2}} \Gamma\left(\frac{D-1}{2}\right)} \int_0^\infty dk \frac{k^{D-3}}{\omega_k} \frac{\sin(k|\Delta x_{\alpha\varrho}|)}{|\Delta x_{\alpha\varrho}|} e^{-i\omega_k \Delta t_{\alpha\varrho}}. \quad (4.4)$$

Using the dispersion relationship $\omega_k^2 = k^2 + m^2$ to replace the integration variable k by ω_k , we obtain

$$G^{(\alpha\varrho)}(\Delta\tau) = \int_m^\infty d\omega_k \frac{\left(\sqrt{\omega_k^2 - m^2}\right)^{D-4}}{|\Delta x_{\alpha\varrho}|} \sin\left(\sqrt{\omega_k^2 - m^2} |\Delta x_{\alpha\varrho}|\right) e^{-i\omega_k \Delta t_{\alpha\varrho}}, \quad (4.5)$$

where $|\Delta x_{\alpha\varrho}| = \sqrt{|x_\alpha - x'_\varrho|}$, $\Delta t_{\alpha\varrho} = t_\alpha - t'_\varrho$.

Now inserting the trajectories (2.2) of two atoms into the expression (4.5), we obtain

$$G^{(11)}(\Delta\tau) = G^{(22)}(\Delta\tau) = \frac{m^{D-2}}{(4\pi)^{\frac{D-1}{2}} \Gamma\left(\frac{D-1}{2}\right)} \int_1^\infty dx (x^2 - 1)^{\frac{D-3}{2}} e^{-i\frac{2}{a} m x \sinh \frac{a\Delta\tau}{2}}, \quad (4.6)$$

and

$$\begin{aligned} G^{(12)}(\Delta\tau) &= G^{(21)}(\Delta\tau) = \\ &= \frac{m^{D-3}}{L(4\pi)^{\frac{D-1}{2}} \Gamma\left(\frac{D-1}{2}\right)} \int_1^\infty dx (x^2 - 1)^{\frac{D-4}{2}} \sin\left(mL(x^2 - 1)^{\frac{1}{2}}\right) e^{-i\frac{2}{a} m x \sinh \frac{a\Delta\tau}{2}}. \end{aligned} \quad (4.7)$$

Further, we can write the expressions (4.6) in the manner of K -Bessel function [58] as

$$G^{(11)}(\Delta\tau) = G^{(22)}(\Delta\tau) = \frac{m^{D-2}}{(4\pi)^{\frac{D-1}{2}} \left(i\frac{m}{a} \sinh\left(\frac{a\Delta\tau}{2}\right)^{\frac{D-2}{2}} \Gamma\left(\frac{1}{2}\right)\right)} K_{\frac{D-2}{2}} \left(i\frac{2m}{a} \sinh\left(\frac{a\Delta\tau}{2}\right)\right) \quad (4.8)$$

where K represents modified Bessel functions of the second kind. But for the off-diagonal terms of the Wightman function, only when $D = 4$, they can be written in the manner of K -Bessel function [58],

$$G^{(12)}(\Delta\tau) = G^{(21)}(\Delta\tau) = \frac{m}{(4\pi)^{\frac{3}{2}} \Gamma\left(\frac{3}{2}\right)} \frac{1}{\sqrt{L^2 - \frac{4}{a^2} \sinh^2\left(\frac{a\Delta\tau}{2}\right)}} K_1 \left(m \sqrt{L^2 - \frac{4}{a^2} \sinh^2\left(\frac{a\Delta\tau}{2}\right)}\right). \quad (4.9)$$

It is found that the Wightman functions for the case considering the massive field can be regarded as the multiplication of a K -Bessel function and the Wightman functions for the case considering the massless field up to a constant related to mass m . Thus, it is not easy to obtain the Fourier transform of the Wightman functions for the case considering the massive field with numerical methods because the absolute values of the argument of

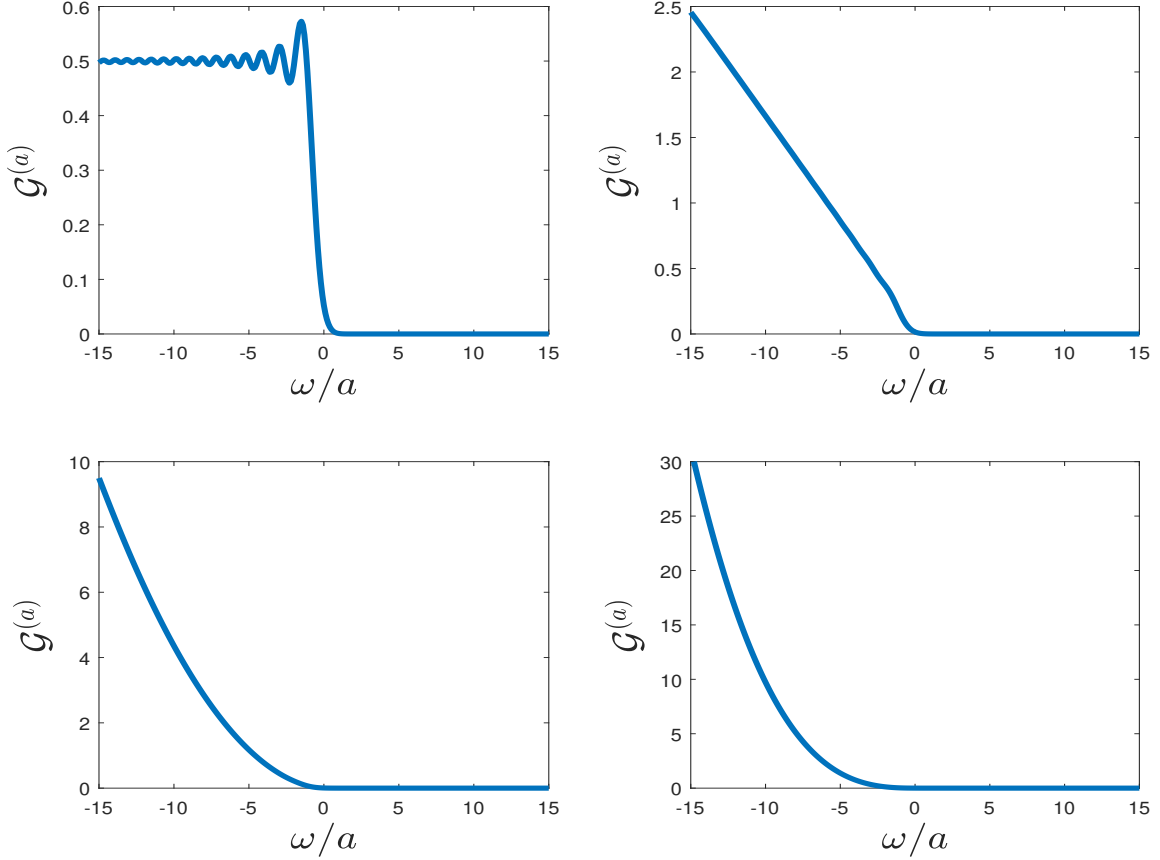


Figure 11. Behavior of $\mathcal{G}^{(a)}$ for massive field in different spacetime dimensions. The four subfigures stand for $D = 3$, $D = 4$, $D = 5$, and $D = 6$, respectively, from left to right and top to bottom.

K -Bessel functions are highly oscillatory. In order to acquire the power spectrum in the case of the massive field, we rewrite the Fourier transform of (4.6) as

$$\mathcal{G}^{(a)} = \frac{am^{D-3}}{(4\pi)^{\frac{D-1}{2}} \Gamma\left(\frac{D-1}{2}\right)} \int_{\frac{m}{a}}^{\infty} dx \left(\frac{a^2}{m^2} x^2 - 1 \right)^{\frac{D-3}{2}} K_{i2\omega/a}(2x), \quad (4.10)$$

and rewrite the Fourier transform of (4.7) as

$$\mathcal{G}^{(b)} = \frac{am^{D-4}}{L(4\pi)^{\frac{D-1}{2}} \Gamma\left(\frac{D-1}{2}\right)} \int_{\frac{m}{a}}^{\infty} dx \left(\frac{a^2}{m^2} x^2 - 1 \right)^{\frac{D-4}{2}} \sin \left[mL \left(\frac{a^2}{m^2} x^2 - 1 \right)^{1/2} \right] K_{i2\omega/a}(2x), \quad (4.11)$$

where we have used the integration formulae

$$\int_{-\infty}^{\infty} e^{-i(2\omega_k) \sinh au/2} e^{i\omega u} du = \frac{4}{a} e^{\frac{\pi\omega}{a}} K_{i2\omega/a}(2\omega_k/a). \quad (4.12)$$

Note that the signs $\mathcal{G}^{(a)}$ and $\mathcal{G}^{(b)}$ represents the Fourier form of the diagonal and off-diagonal terms for the Wightman functions.

Figure 11 and figure 12 show the power spectra in the case of massive field in arbitrary spacetime dimensions by numerical integrating (4.10) and (4.11). Because of the modification

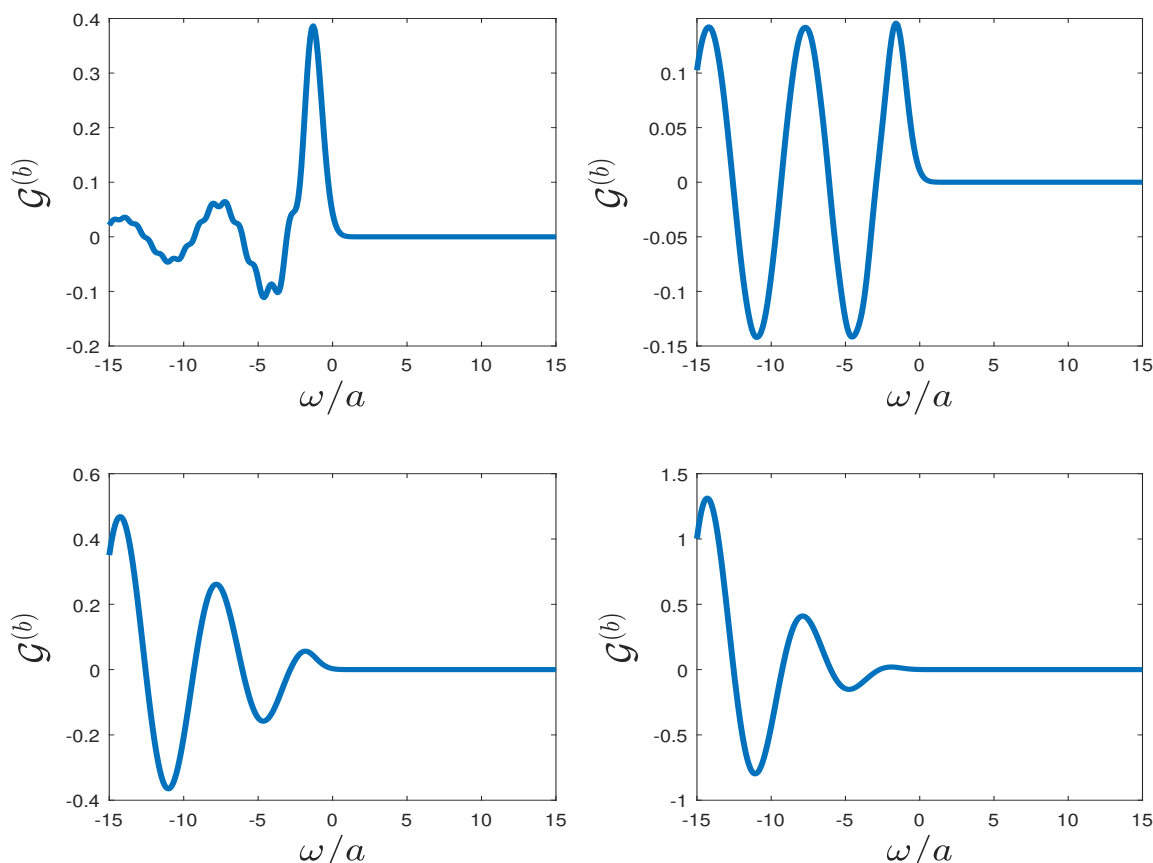


Figure 12. Behavior of $\mathcal{G}^{(b)}$ for massive field in different spacetime dimensions. The four subfigures stand for $D = 3$, $D = 4$, $D = 5$, and $D = 6$, respectively, from left to right and top to bottom.

of K -Bessel functions, all power spectra for the diagonal terms decrease to zero gradually for any spacetime dimension D , but it is special for the $D = 3$ case that including the oscillation in the axis of negative frequency and differs from that for other spacetime dimensions, as given in figure 11. For the off-diagonal terms as given in figure 12, the oscillation for the curves of the power spectra in different spacetime dimensions has the same trend with the in figure 2 for the case of massless field but the period of oscillation becomes larger for the case of massive field due to the modulation of K -Bessel functions. Note that the power spectra of off-diagonal terms for $D = 3$ is also special, which, together with the case of diagonal terms, derives from the function of statistical effect, as discussed in the case of massless field. But for $D = 4$, the statistical effect is not evident for the case of massive field, which is covered in the K -Bessel function. For $D > 4$, the behaviors of the power spectra for the cases of massless and massive field looks similar because the statistical factor in these cases doesn't dominate.

4.2 Entanglement change

Adopting the method of the master equation described in the last section but the power spectra are used with eq. (4.10) and (4.11), we calculate entanglement dynamics of two

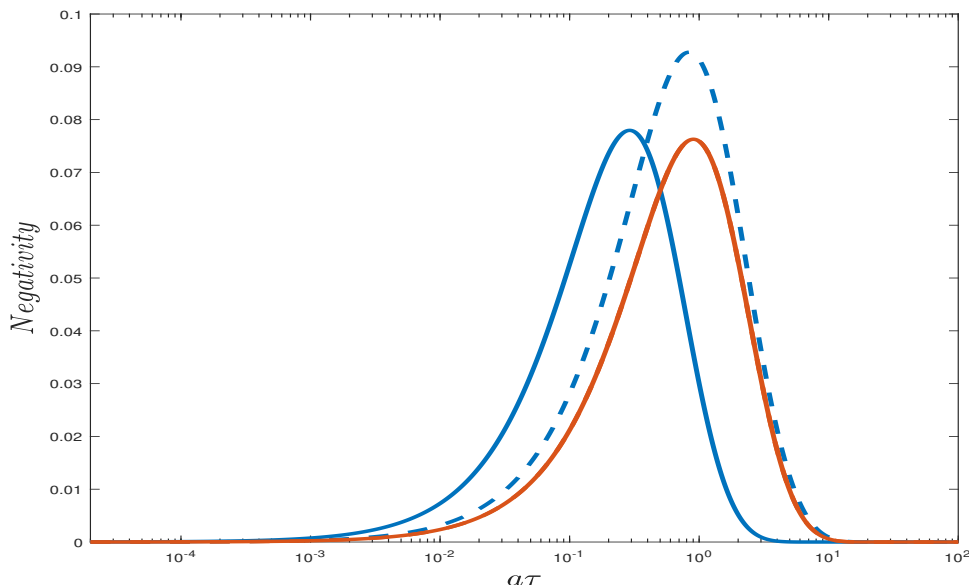


Figure 13. Entanglement evolutionary process over time for massive field. Blue and red lines stand for $D = 3$ and $D = 4$, respectively. Solid and dashed lines stand for the cases of massless and massive field, respectively.

accelerated atoms with the initial product state for the case of the massive field under the different spacetime dimensions. Figure 13 presents the evolution of entanglement with time with the other parameters taking $L, \omega, m = 1$ for the cases of the massless and massive field. By comparison, the entanglement evolution in the case of massive field is always slower, which is an interesting time-delay phenomenon. It seems that the speed of the massive field to propagate the interaction information between two accelerated atoms is slower than that of massless field. Another interesting phenomenon for the case of massive field is that the maximal amount of generated entanglement decrease more quickly when the spacetime dimension D increases than that for the case of massless field. The cases for $D = 5$ and $D = 6$ are consistent with these discussions here and don't present any abnormal behaviors, so we don't plot them in figure 13.

Finally, let's discuss the anti-Unruh effect in different spacetime dimensions. For this, we add an extra Gauss switching function $\chi(\tau) = e^{-\tau^2/2\sigma^2}$ as made in refs. [31, 32] and calculate the Fourier transformation as

$$\mathcal{G}^{(a)} = \int d\tau d\tau' G(\tau, \tau') e^{-i\omega(\tau - \tau')} \chi(\tau) \chi(\tau'). \quad (4.13)$$

For simplicity, we take $\tau' = 0$ here, and obtain

$$\mathcal{G}^{(a)} = \int d\tau G(\tau) e^{-i\omega\tau} \chi(\tau). \quad (4.14)$$

This equation is proportional to the transition probability of an Unruh-Dewitt detector [31, 32]. Inserting eq. (4.8) into eq. (4.14), we can integrate and obtain the power spectrum by employing numerical methods (the oscillatory phenomenon we mentioned before does not

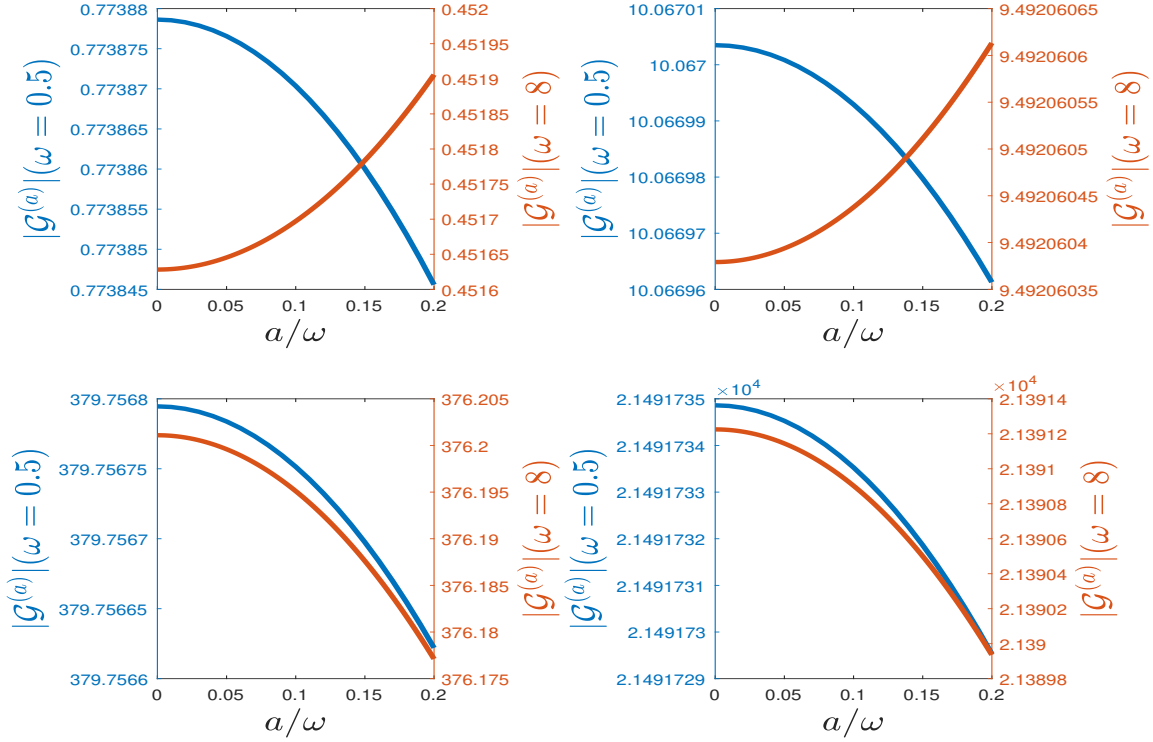


Figure 14. Anti-Unruh effect in different spacetime dimensions. The four subfigures stand for $D = 3$, $D = 4$, $D = 5$, and $D = 6$, respectively, from left to right and top to bottom. Blue and red lines stand for $\omega = 0.5$ and $\omega = 8$, respectively, with other parameters taking $m = 1$, $\sigma = 0.8$.

matter now, because the Gaussian function has suppressed the oscillation to a very low level). The integral range was chosen as $[-10\sigma, 10\sigma]$ ($\sigma = 0.8$) to suppress the numerical error at level of $e^{-50} \sim 10^{-22}$ due to the finite integration range. Figure 14 presents the change of $G^{(a)}$ with acceleration and the anti-Unruh effect is feasible in any spacetime dimension. Interestingly, the anti-Unruh effect is robust to the influence of the spacetime dimensions. But for the Unruh effect in the $D = 3$ and $D = 4$ cases, it changes into the anti-Unruh effect in the $D = 5$ and $D = 6$ cases with the same parameters. This is a remarkable influence from the spacetime dimensions but the fundamentally physical reason is unclear now and remains to be explored in the future. In fact, the fundamentally physical reason for the appearance of anti-Unruh effect is not clear up to now although the required conditions has been discussed many times [31, 32, 36–41].

5 Conclusion

In this paper, we have investigated the entanglement dynamics of a quantum system composed of two uniformly accelerated Unruh-DeWitt detectors coupled with both fluctuating massless and massive field in an arbitrary dimensional Minkowski vacuum. The main results focused on the influence of the spacetime dimensions on the change of entanglement.

At first, we investigate the behaviors of the power spectrum for different spacetime dimensions. For the case of the massless field, the power spectrum obeys Bose-Einstein

distribution in even dimensions, and Fermi-Dirac distribution in odd dimensions. For diagonal components, the power spectrum completely obeys Fermi-Dirac distribution when $D = 3$, but has to be regarded as the multiplication of a polynomial multiplication term and a Bose/Fermi factor when $D \geq 4$ in which the statistical effect doesn't dominate. For off-diagonal components, the power spectrum can be regarded as the multiplication of the corresponding power spectrum for diagonal components and a hypergeometric function. The power spectra for off-diagonal components present the oscillating behavior with ω but differs for different spacetime dimensions.

Then, the influence of spacetime dimensions on change of entanglement between two accelerated atoms is studied in the case of the massless field. Considering an initial product state for two atoms, the acceleration leads to the generation of entanglement between two atoms. It is found that the range of the parameters (ω, L, a) in which entanglement between two atoms can be generated is shrunk with increasing spacetime dimension D , which is measured by the area of entanglement region from figure 3 to figure 6. Meanwhile, the maximal amount of generated entanglement decreases with increasing D , which is seen by the entanglement evolution with time in figure 7. We also study the change of generated maximal entanglement with acceleration for different atom separations and find that for the proper separation between two atoms, entanglement can be enhanced for a certain range of increasing acceleration, which is similar to the anti-Unruh effect, but this phenomenon doesn't appear at the same separation for different spacetime dimensions and it appears at smaller separation for lower spacetime dimensions. When L is large enough, the maximal entanglement will oscillate with increasing acceleration, which shows that the generated entanglement is unstable and very small. When L is increased further ($\rightarrow \infty$), the entanglement will decrease very quickly to zeros in any spacetime dimensions. When the two atoms are placed at the same places ($L \rightarrow 0$), entanglement is generated to the maximal value at some certain ω , remains there for a certain range of ω , and then decreases to zero suddenly at another certain ω . Note that these certain ω is dependent on the spacetime dimensions. Moreover, the change of entanglement for the initial entangled state of two atom is also studied, and the difference of entanglement change with time for different spacetime dimensions are presented with different initial entangled states for two atoms.

Finally, we expand the discussion to the case of the massive field. The Wightman functions and the power spectra are obtained by adding an extra factor expressed by K-Bessel functions in the basis of the results for the case of the massless field. When entanglement evolution is calculated in this case, it is found that mass can lead to a time delay for entanglement generation in any spacetime dimensions, compared with that for the case of the massless field. But the generated maximal entanglement decreases more quickly with increasing spacetime dimension than that for the case of massless field. When we study the change of generated maximal entanglement with the acceleration, a surprised and attractive result is found that the Unruh effect in the small spacetime dimensions can change to the anti-Unruh effect in large spacetime dimensions with the same other parameters.

Acknowledgments

This work is supported by the NSFC Grant Nos. 11654001.

Open Access. This article is distributed under the terms of the Creative Commons Attribution License ([CC-BY 4.0](https://creativecommons.org/licenses/by/4.0/)), which permits any use, distribution and reproduction in any medium, provided the original author(s) and source are credited. SCOAP³ supports the goals of the International Year of Basic Sciences for Sustainable Development.

References

- [1] W.G. Unruh, *Notes on black hole evaporation*, *Phys. Rev. D* **14** (1976) 870 [[INSPIRE](#)].
- [2] P.C.W. Davies, *Scalar particle production in Schwarzschild and Rindler metrics*, *J. Phys. A* **8** (1975) 609 [[INSPIRE](#)].
- [3] S.A. Fulling, *Nonuniqueness of canonical field quantization in Riemannian space-time*, *Phys. Rev. D* **7** (1973) 2850 [[INSPIRE](#)].
- [4] L.C.B. Crispino, A. Higuchi and G.E.A. Matsas, *The Unruh effect and its applications*, *Rev. Mod. Phys.* **80** (2008) 787 [[arXiv:0710.5373](#)] [[INSPIRE](#)].
- [5] M. Chernicoff and A. Paredes, *Accelerated detectors and worldsheet horizons in AdS/CFT*, *JHEP* **03** (2011) 063 [[arXiv:1011.4206](#)] [[INSPIRE](#)].
- [6] J.G. Russo and P.K. Townsend, *Accelerating Branes and Brane Temperature*, *Class. Quant. Grav.* **25** (2008) 175017 [[arXiv:0805.3488](#)] [[INSPIRE](#)].
- [7] A.A. Saharian, *Wightman function and vacuum fluctuations in higher dimensional brane models*, *Phys. Rev. D* **73** (2006) 044012 [[hep-th/0508038](#)] [[INSPIRE](#)].
- [8] J. Audretsch and R. Muller, *Radiative energy shifts of accelerated atoms*, *Phys. Rev. A* **52** (1995) 629 [[gr-qc/9503058](#)] [[INSPIRE](#)].
- [9] R. Passante, *Radiative level shifts of an accelerated hydrogen atom and the Unruh effect in quantum electrodynamics*, *Phys. Rev. A* **57** (1998) 1590.
- [10] L. Rizzuto et al., *Nonthermal effects of acceleration in the resonance interaction between two uniformly accelerated atoms*, *Phys. Rev. A* **94** (2016) 012121 [[arXiv:1601.04502](#)] [[INSPIRE](#)].
- [11] W. Zhou, R. Passante and L. Rizzuto, *Resonance interaction energy between two accelerated identical atoms in a coaccelerated frame and the Unruh effect*, *Phys. Rev. D* **94** (2016) 105025 [[arXiv:1609.06931](#)] [[INSPIRE](#)].
- [12] I. Fuentes-Schuller and R.B. Mann, *Alice falls into a black hole: Entanglement in non-inertial frames*, *Phys. Rev. Lett.* **95** (2005) 120404 [[quant-ph/0410172](#)] [[INSPIRE](#)].
- [13] Y. Dai, Z. Shen and Y. Shi, *Killing quantum entanglement by acceleration or a black hole*, *JHEP* **09** (2015) 071 [[arXiv:1507.00612](#)] [[INSPIRE](#)].
- [14] P.M. Alsing, I. Fuentes-Schuller, R.B. Mann and T.E. Tessier, *Entanglement of Dirac fields in non-inertial frames*, *Phys. Rev. A* **74** (2006) 032326 [[quant-ph/0603269](#)] [[INSPIRE](#)].
- [15] E. Martin-Martinez and J. Leon, *Are Alice and Rob really protected by statistics as she falls into a black hole?*, *Phys. Rev. A* **80** (2009) 042318 [[arXiv:0907.1960](#)] [[INSPIRE](#)].
- [16] E. Martin-Martinez, L.J. Garay and J. Leon, *Unveiling quantum entanglement degradation near a Schwarzschild black hole*, *Phys. Rev. D* **82** (2010) 064006 [[arXiv:1006.1394](#)] [[INSPIRE](#)].
- [17] J. Wang and J. Jing, *Multipartite entanglement of fermionic systems in noninertial frames*, *Phys. Rev. A* **83** (2011) 022314 [Erratum *ibid.* **97** (2018) 029902] [[arXiv:1012.4268](#)] [[INSPIRE](#)].

- [18] M. Shamirzai, B.N. Esfahani and M. Soltani, *Tripartite Entanglements in Non-inertial Frames*, *Int. J. Theor. Phys.* **51** (2012) 787 [[arXiv:1103.0258](#)] [[INSPIRE](#)].
- [19] D.E. Bruschi, A. Dragan, I. Fuentes and J. Louko, *Particle and anti-particle bosonic entanglement in non-inertial frames*, *Phys. Rev. D* **86** (2012) 025026 [[arXiv:1205.5296](#)] [[INSPIRE](#)].
- [20] B. Richter and Y. Omar, *Degradation of entanglement between two accelerated parties: Bell states under the Unruh effect*, *Phys. Rev. A* **92** (2015) 022334 [[arXiv:1503.07526](#)] [[INSPIRE](#)].
- [21] J. Hu and H. Yu, *Entanglement dynamics for uniformly accelerated two-level atoms*, *Phys. Rev. A* **91** (2015) 012327 [[arXiv:1501.03321](#)] [[INSPIRE](#)].
- [22] B. Reznik, A. Retzker and J. Silman, *Violating Bell's inequalities in the vacuum*, *Phys. Rev. A* **71** (2005) 042104 [[quant-ph/0310058](#)] [[INSPIRE](#)].
- [23] G.L. Ver Steeg and N.C. Menicucci, *Entangling power of an expanding universe*, *Phys. Rev. D* **79** (2009) 044027 [[arXiv:0711.3066](#)] [[INSPIRE](#)].
- [24] M. Montero and E. Martin-Martinez, *The entangling side of the Unruh-Hawking effect*, *JHEP* **07** (2011) 006 [[arXiv:1011.6540](#)] [[INSPIRE](#)].
- [25] B.S. DeWitt, S. Hawking and W. Israel, *General relativity: an Einstein centenary survey*, Cambridge Press, Cambridge U.K. (1979).
- [26] B. Reznik, *Entanglement from the vacuum*, *Found. Phys.* **33** (2003) 167 [[quant-ph/0212044](#)] [[INSPIRE](#)].
- [27] W. Cong, E. Tjoa and R.B. Mann, *Entanglement Harvesting with Moving Mirrors*, *JHEP* **06** (2019) 021 [Erratum *ibid.* **07** (2019) 051] [[arXiv:1810.07359](#)] [[INSPIRE](#)].
- [28] J. Zhang and H. Yu, *Entanglement harvesting for Unruh-DeWitt detectors in circular motion*, *Phys. Rev. D* **102** (2020) 065013 [[arXiv:2008.07980](#)] [[INSPIRE](#)].
- [29] K. Gallock-Yoshimura, E. Tjoa and R.B. Mann, *Harvesting entanglement with detectors freely falling into a black hole*, *Phys. Rev. D* **104** (2021) 025001 [[arXiv:2102.09573](#)] [[INSPIRE](#)].
- [30] P. Chowdhury and B.R. Majhi, *Fate of entanglement between two Unruh-DeWitt detectors due to their motion and background temperature*, *JHEP* **05** (2022) 025 [[arXiv:2110.11260](#)] [[INSPIRE](#)].
- [31] W.G. Brenna, R.B. Mann and E. Martin-Martinez, *Anti-Unruh Phenomena*, *Phys. Lett. B* **757** (2016) 307 [[arXiv:1504.02468](#)] [[INSPIRE](#)].
- [32] L.J. Garay, E. Martin-Martinez and J. de Ramon, *Thermalization of particle detectors: The Unruh effect and its reverse*, *Phys. Rev. D* **94** (2016) 104048 [[arXiv:1607.05287](#)] [[INSPIRE](#)].
- [33] R. Kubo, *Statistical-mechanical theory of irreversible processes. I. General theory and simple applications to magnetic and conduction problems*, *J. Phys. Soc. Jpn.* **12** (1957) 570.
- [34] P.C. Martin and J.S. Schwinger, *Theory of many particle systems. I*, *Phys. Rev.* **115** (1959) 1342 [[INSPIRE](#)].
- [35] C.J. Fewster, B.A. Juárez-Aubry and J. Louko, *Waiting for Unruh*, *Class. Quant. Grav.* **33** (2016) 165003 [[arXiv:1605.01316](#)] [[INSPIRE](#)].
- [36] T. Li, B. Zhang and L. You, *Would quantum entanglement be increased by anti-Unruh effect?*, *Phys. Rev. D* **97** (2018) 045005 [[arXiv:1802.07886](#)] [[INSPIRE](#)].

- [37] Y. Zhou, J. Hu and H. Yu, *Entanglement dynamics for Unruh-DeWitt detectors interacting with massive scalar fields: the Unruh and anti-Unruh effects*, *JHEP* **09** (2021) 088 [[arXiv:2105.14735](#)] [[INSPIRE](#)].
- [38] Y. Chen, J. Hu and H. Yu, *Entanglement generation for uniformly accelerated atoms assisted by environment-induced interatomic interaction and the loss of the anti-Unruh effect*, *Phys. Rev. D* **105** (2022) 045013 [[arXiv:2110.01780](#)] [[INSPIRE](#)].
- [39] Y. Pan and B. Zhang, *Influence of acceleration on multibody entangled quantum states*, *Phys. Rev. A* **101** (2020) 062111 [[arXiv:2009.05179](#)] [[INSPIRE](#)].
- [40] Y. Pan and B. Zhang, *Anti-Unruh effect in the thermal background*, *Phys. Rev. D* **104** (2021) 125014 [[arXiv:2112.01889](#)] [[INSPIRE](#)].
- [41] S. Barman and B.R. Majhi, *Radiative process of two entangled uniformly accelerated atoms in a thermal bath: a possible case of anti-Unruh event*, *JHEP* **03** (2021) 245 [[arXiv:2101.08186](#)] [[INSPIRE](#)].
- [42] M. Bañados, C. Teitelboim and J. Zanelli, *The Black hole in three-dimensional space-time*, *Phys. Rev. Lett.* **69** (1992) 1849 [[hep-th/9204099](#)] [[INSPIRE](#)].
- [43] L.J. Henderson, R.A. Hennigar, R.B. Mann, A.R.H. Smith and J. Zhang, *Anti-Hawking phenomena*, *Phys. Lett. B* **809** (2020) 135732 [[arXiv:1911.02977](#)] [[INSPIRE](#)].
- [44] M.P.G. Robbins, L.J. Henderson and R.B. Mann, *Entanglement amplification from rotating black holes*, *Class. Quant. Grav.* **39** (2021) 02LT01.
- [45] Y. Dai, Z. Shen and Y. Shi, *Quantum entanglement in three accelerating qubits coupled to scalar fields*, *Phys. Rev. D* **94** (2016) 025012 [[arXiv:1512.04886](#)] [[INSPIRE](#)].
- [46] J. Wang, L. Zhang, S. Chen and J. Jing, *Estimating the Unruh effect via entangled many-body probes*, *Phys. Lett. B* **802** (2020) 135239 [[arXiv:2001.07865](#)] [[INSPIRE](#)].
- [47] S. Takagi, *Vacuum Noise and Stress Induced by Uniform Acceleration: Hawking-Unruh Effect in Rindler Manifold of Arbitrary Dimension*, *Prog. Theor. Phys. Suppl.* **88** (1986) 1 [[INSPIRE](#)].
- [48] L. Sriramkumar, *Odd statistics in odd dimensions for odd couplings*, *Mod. Phys. Lett. A* **17** (2002) 1059 [[gr-qc/0206048](#)] [[INSPIRE](#)].
- [49] S. Ohya, *Emergent Anyon Distribution in the Unruh Effect*, *Phys. Rev. D* **96** (2017) 045017 [[arXiv:1706.03761](#)] [[INSPIRE](#)].
- [50] J. Hu and H. Yu, *Geometric phase for an accelerated two-level atom and the Unruh effect*, *Phys. Rev. A* **85** (2012) 032105 [[arXiv:1203.5869](#)] [[INSPIRE](#)].
- [51] J. Feng, J.-J. Zhang and Q. Zhang, *Geometric phase under the Unruh effect with intermediate statistics*, *Chin. Phys. B* **31** (2022) 050312 [[INSPIRE](#)].
- [52] J. Feng and J.-J. Zhang, *Quantum Fisher information as a probe for Unruh thermality*, *Phys. Lett. B* **827** (2022) 136992 [[arXiv:2111.00277](#)] [[INSPIRE](#)].
- [53] J. Rodriguez-Laguna, L. Tarruell, M. Lewenstein and A. Celi, *Synthetic Unruh effect in cold atoms*, *Phys. Rev. A* **95** (2017) 013627 [[arXiv:1606.09505](#)] [[INSPIRE](#)].
- [54] A. Kosior, M. Lewenstein and A. Celi, *Unruh effect for interacting particles with ultracold atoms*, *SciPost Phys.* **5** (2018) 061 [[arXiv:1804.11323](#)] [[INSPIRE](#)].
- [55] H.-P. Breuer and F. Petruccione, *The theory of open quantum systems*, Oxford University Press, Oxford U.K. (2007) [[DOI](#)].

- [56] G. Kaplanek and C.P. Burgess, *Hot Accelerated Qubits: Decoherence, Thermalization, Secular Growth and Reliable Late-time Predictions*, *JHEP* **03** (2020) 008 [[arXiv:1912.12951](#)] [[INSPIRE](#)].
- [57] J. Arrechea, C. Barceló, L.J. Garay and G. García-Moreno, *Inversion of statistics and thermalization in the Unruh effect*, *Phys. Rev. D* **104** (2021) 065004 [[arXiv:2101.11933](#)] [[INSPIRE](#)].
- [58] A. Jeffrey and D. Zwillinger, eds, *Table of integrals, series, and products*, Academic Press, Elsevier, Burlington U.S.A. (2007).
- [59] R.H. Dicke, *Coherence in Spontaneous Radiation Processes*, *Phys. Rev.* **93** (1954) 99 [[INSPIRE](#)].
- [60] G. Vidal and R.F. Werner, *Computable measure of entanglement*, *Phys. Rev. A* **65** (2002) 032314 [[quant-ph/0102117](#)] [[INSPIRE](#)].
- [61] K. Zyczkowski, P. Horodecki, A. Sanpera and M. Lewenstein, *On the volume of the set of mixed entangled states*, *Phys. Rev. A* **58** (1998) 883 [[quant-ph/9804024](#)] [[INSPIRE](#)].
- [62] A. Peres, *Separability criterion for density matrices*, *Phys. Rev. Lett.* **77** (1996) 1413 [[quant-ph/9604005](#)] [[INSPIRE](#)].
- [63] L.-L. Chau and D.-W. Huang, *Ising fluctuations for the intermittent and scaling behaviors of high-energy multiparticle productions*, *Phys. Lett. B* **283** (1992) 1 [[INSPIRE](#)].